Double ratio method for the binding energies of hypernuclei in nuclear reactions

Nihal Buyukcizmeci,
Selçuk University, Department of Physics, 42079, Konya, Turkey

(in collaboration with A.S.Botvina, M. Bleicher, A. Kaya and R. Ogul)
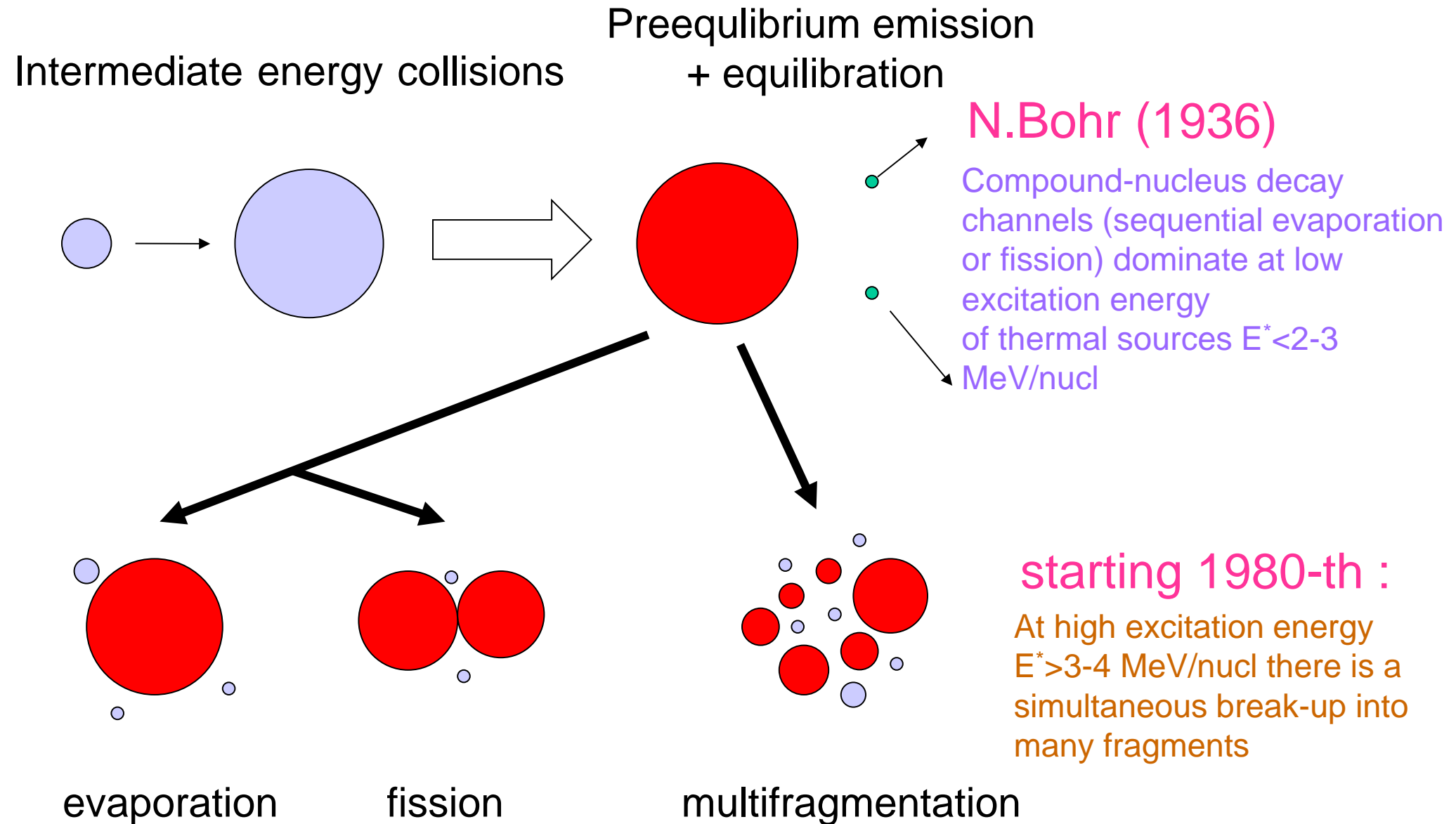
COST CA15213 THOR Annual Meeting,
September 2-6, 2019, Istanbul, Turkey.

- Relativistic collisions of ions, hadrons and leptons with nuclei can produce various hypernuclei by the capture of hyperons in nuclear residues.

- The disintegration of such hypernuclear systems can be described with statistical approaches suggesting that the fragment production is related to the binding energies of hypernuclei.

- We demonstrate how the hyperon binding energies can be effectively evaluated from the yields of different hyper-isotopes using the double ratio method.

Statistical approach in nuclear reactions: conception of equilibrium

Intermediate energy collisions

Preequlibrium emission
+ equilibration

N.Bohr (1936)

Compound-nucleus decay channels (sequential evaporation or fission) dominate at low excitation energy
of thermal sources $E^* < 2$-3 MeV/nucl

starting 1980-th :

At high excitation energy $E^* > 3$-4 MeV/nucl there is a simultaneous break-up into many fragments

evaporation   fission   multifragmentation

V.Weisskopf (1937) N.Bohr, J.Wheeler (1939) Bondorf et al. (1995) SMM

Evaporation from hot fragments

The successive particle emission from hot primary fragments with A>16 is assumed to be their basic de-excitation mechanism. Due to the high excitation energy of these fragments, standard Weisskopf evaporation scheme [2] was modified to take into account the heavier ejectiles up to ^{18}O, besides light particles (nucleons, d, t, α), in ground and particle-stable excited states [81]. This corresponds to the excitation energies $\epsilon^{(i)}$ of the ejectiles not higher than 7-8 MeV. By analogy with standard model **the width for the emission of a particle j from the compound nucleus (A,Z) is given by:**

$$\Gamma_j = \sum_{i=1}^{n} \int_0^{E_{AZ}^* - B_j - \epsilon_j^{(i)}} \frac{\mu_j g_j^{(i)}}{\pi^2 \hbar^3} \sigma_j(E) \frac{\rho_{A'Z'}(E_{AZ}^* - B_j - E)}{\rho_{AZ}(E_{AZ}^*)} E dE$$

Here the sum is taken over the ground and all particle-stable excited states $\epsilon_j^{(i)}$ (i=0,1,...n) of the fragment j, $g_j^{(i)}=(2s_j^{(i)}+1)$ is the spin degeneracy factor of the ith excited state, μ_j and B_j are corressponding reduced mass and seperation energy, E_{AZ}^* is the excitation energy of the initial nucleus (55), E is the kinetic energy of an emitted particle in the centre of mass frame. ρ_{AZ} and $\rho_{A'Z'}$ are the level densities of the initial (A,Z) and final (A',Z') compound nuclei. calculated using the Fermi-gas formula. The cross section σ_j (E) of the inverse reaction (A',Z')+j=(A,Z) was calculated using the optical model with nucleus-nucleus potential. The evaporational process was simulated by the Monte Carlo method using the algorithm described in Ref.[118]. The conservation of energy and momentum was strictly controlled in each emission step.

Nuclear fission

An important channel of de-excitation of heavy nuclei (A>200) is fission. This process competes with particle emission. Following the Bohr-Wheeler statistical approach we assume that the **partial width for the compound nucleus fission is propotional to the level density at the saddle point** $\rho_{sp}(E)$ [1]:

$$\Gamma_j = \frac{1}{2\pi\rho_{AZ}(E^*_{AZ})} \int\limits_0^{E^*_{AZ}-B_j} \rho_{sp}(E^*_{AZ} - B_j - E)dE \ ,$$

where B_f is the height of the fission barrier which is determined by the Myers-Swiatecki prescription [120]. For approximation of ρ_{sp} we used the results of the extensive analysis of nuclear fissibility and Γ_s/Γ_f branching ratios [121]. The influence of the shell structure on the level densities ρ_{sp} and ρ_{AZ} is disregarded since in the case of multifragmentation we are dealing with very high excitation energies E*>30-50 MeV when shell effects are expected to be washed out [122].
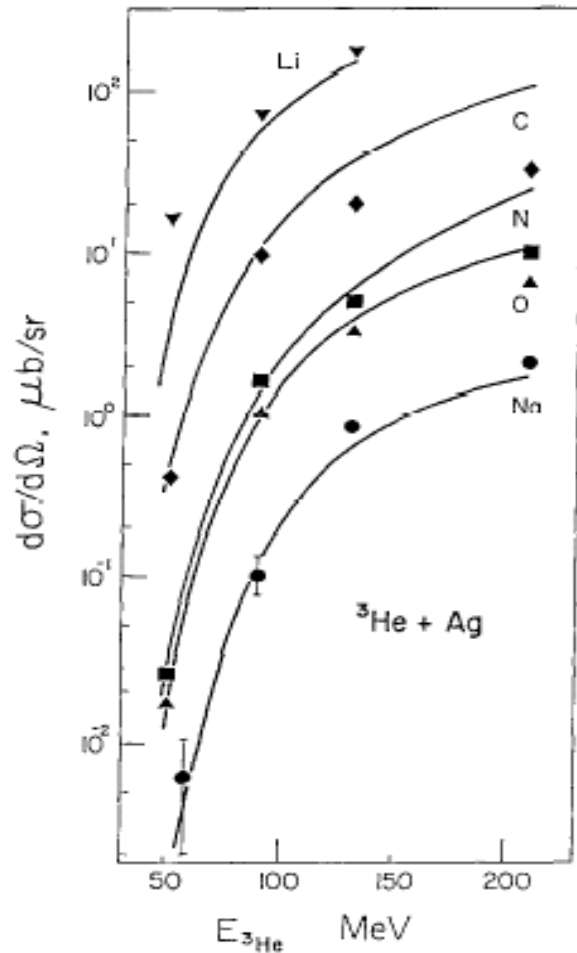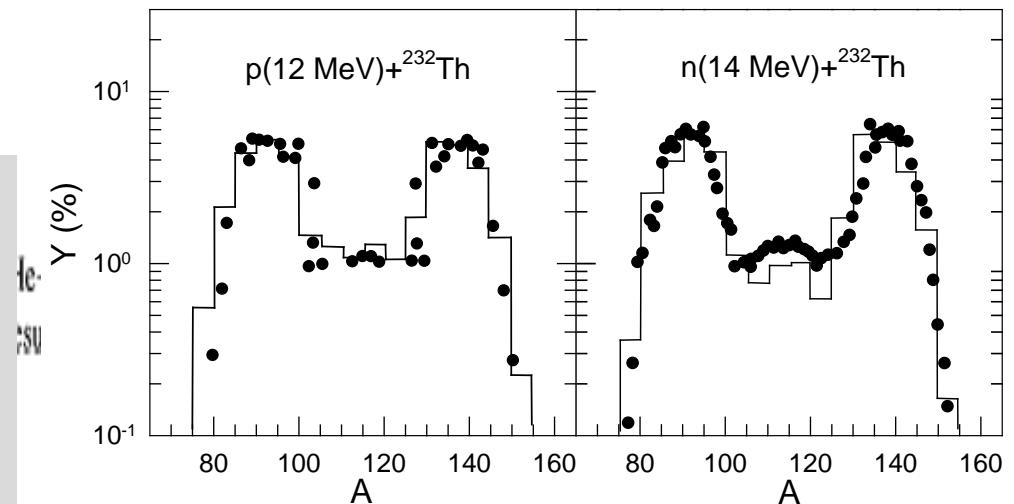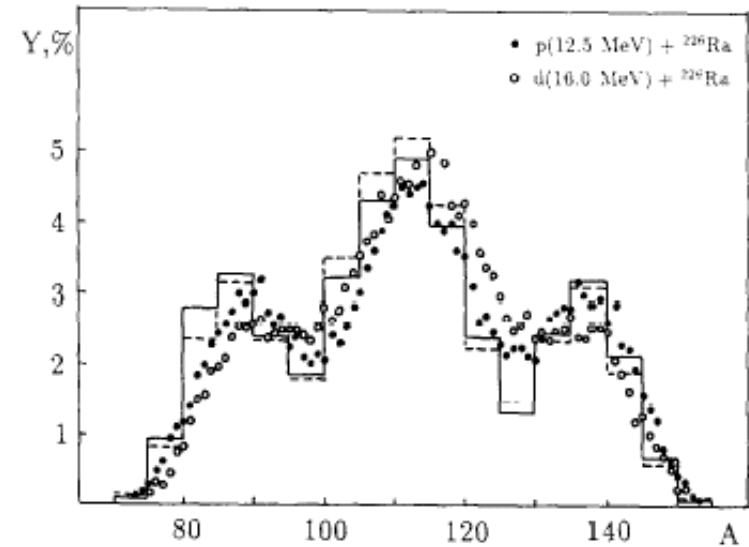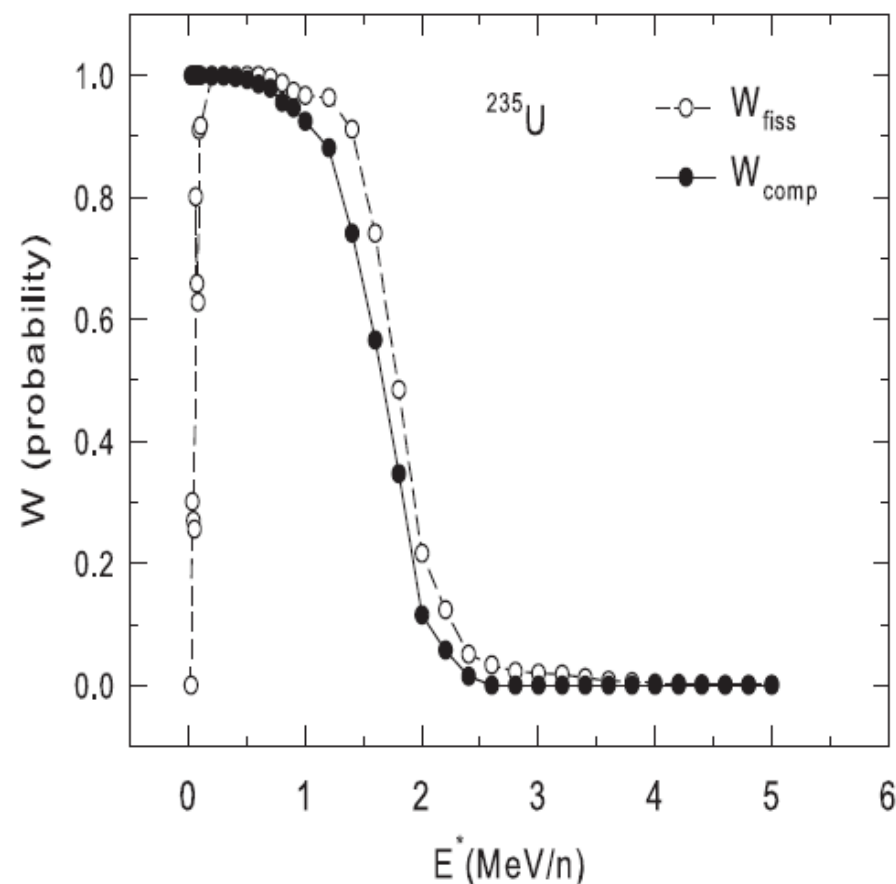
sequential evaporation of fragments

Fig. 4.1. Cross section for heavy cluster emission at backward angles (θ=120-160º) in the reaction ^{3}He+Ag as a function of the laboratory kinetic energy of ^{3}He. The data are from Ref.[119], and the curves show the results of the evaporation model calculation described in the text.
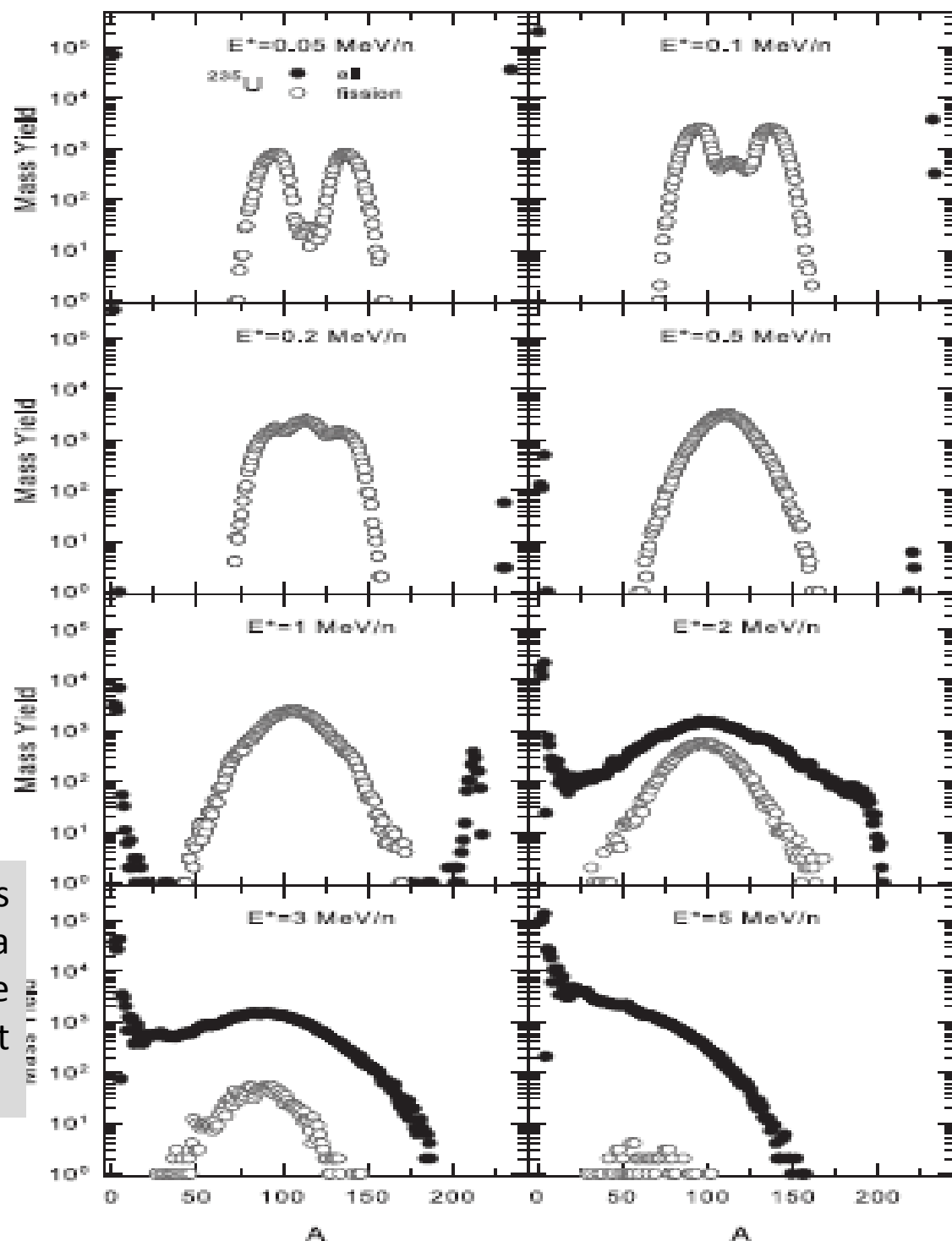
nuclear fission
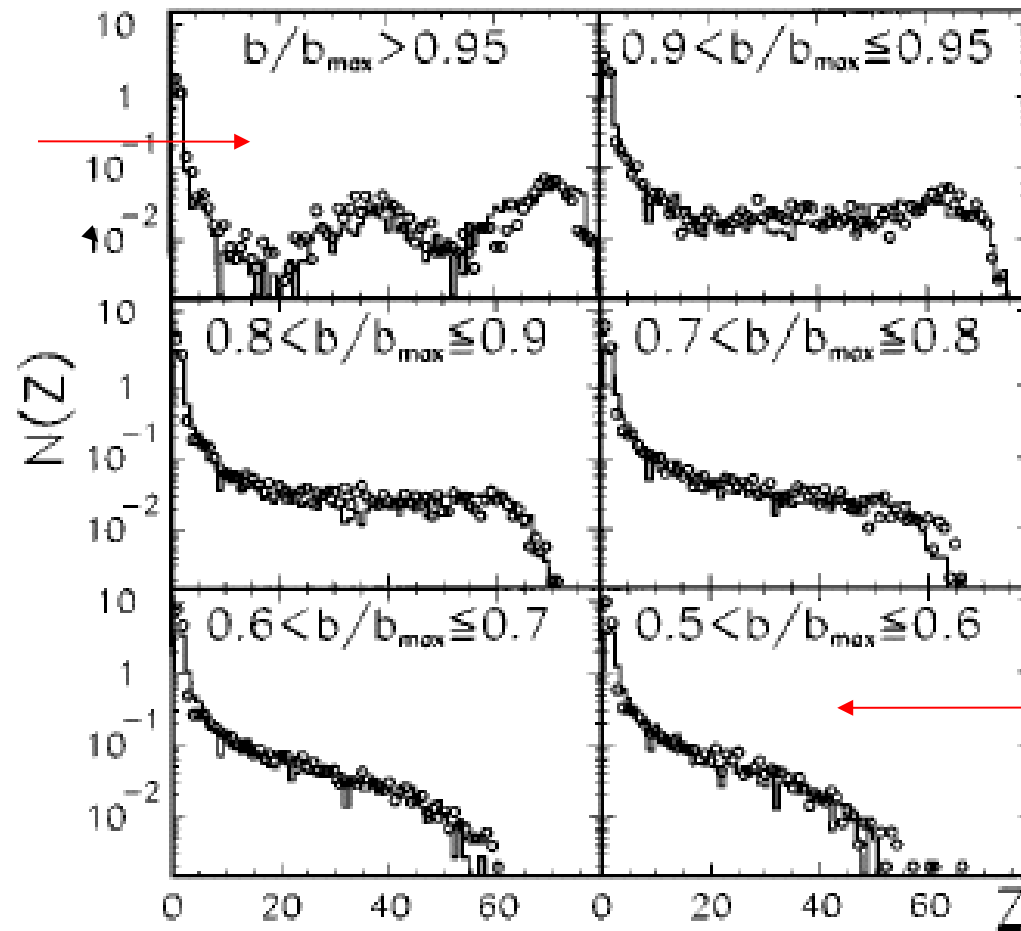
Survival probability of the compound nucleus Wcomp and fission probability Wfiss as a function of the excitation energy, for the disintegration of ^{235}U as obtained in the present SMM calculations.

MULTICS

Au(35MeV/N)+Au, peripheral

2 MeV/n →

5 MeV/n ←

Fig.8. Charge distributions for peripheral and midperipheral collisions (open point:experimental data; histogram:SMM predictions).

Multifragmentation versus sequential evaporation

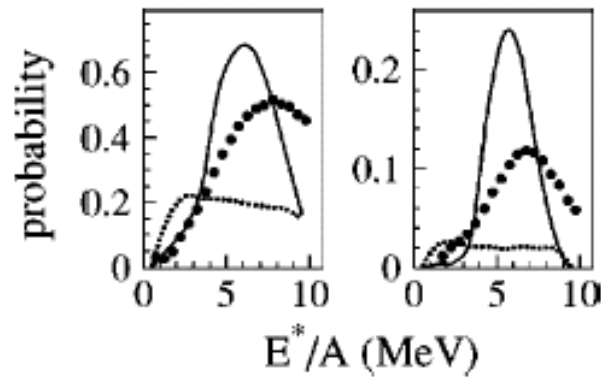**ISIS**   π⁻(8GeV/c)+Au

ALADIN   Au (600 MeV/n) +X.

FIG. 3. Left panel: dots present the raw measured probability to detect an event with at least one heavy-fragment, $Z \geq 8$, and solid (dotted) line presents the SMM (GEMINI) model prediction filtered with the experimental detection efficiency. An initial angular momentum of $L = 20\hbar$ for the hot nucleus was assumed for GEMINI model calculations. Right panel: as in left panel, but for the probability of detecting events with at least two heavy-fragments, $Z \geq 8$.
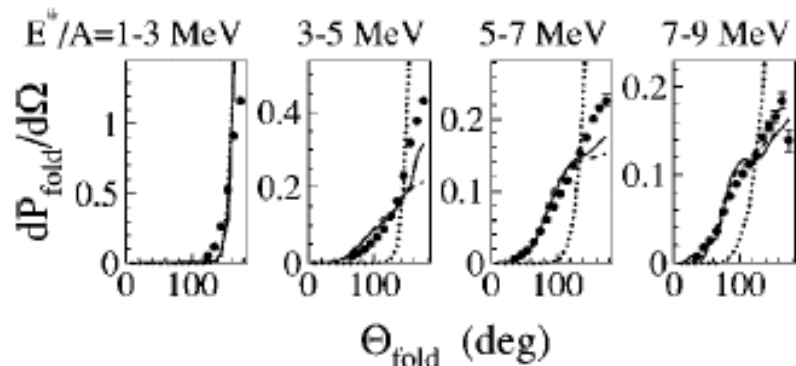

FIG. 2. The measured folding-angle (the angle between two $Z \geq 8$ fragments) probability for the indicated excitation-energy bins. Solid, dashed, and dotted lines show the SMM-hot, SMM-cold, and GEMINI model predictions, respectively, filtered with the experimental detection efficiency.
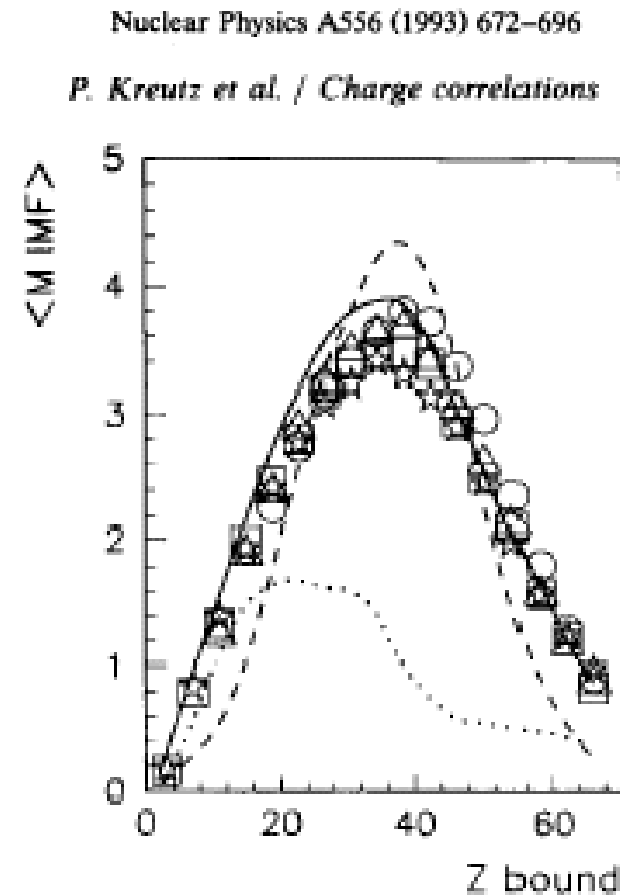
Nuclear Physics A556 (1993) 672–696

P. Kreutz et al. / Charge correlations

Fig. 15. The average multiplicity of IMFs as a function of Z_{bound} for Au 600 MeV/nucleon collisions on C (circles), Al (triangles), Cu (squares) and Pb (stars). The error bars are in most cases smaller than the size of the symbols. The lines are COPENHAGEN (dashed), GEMINI (dotted) and percolation (full) predictions.

The Fermi break-up

For light primary fragments (with A≤ 16) even a relatively small excitation energy may be comparable with their total binding energy. In this case we assume that the principal mechanism old deexcitation is the explosive decay of the excited nucleus into several smaller clusters (the seconday break-up). To describe this process we use the famous Fermi model. It is analogous to the above-described statistical model, but all final-stage fragments are assumed to be in their ground or low excited states. In this case the statistical weight of the channel containing n particles with masses mi(i:1,...n) in volüme Vf may be calculated in microcanonical approximation:

$$\Delta\Gamma_f^{mic} \propto \frac{S}{G}\left(\frac{V_f}{(2\pi\hbar)^3}\right)^{n-1}\left(\frac{\prod_{i=1}^n m_i}{m_0}\right)^{3/2}\frac{(2\pi)^{(3/2)(n-1)}}{\Gamma(\frac{3}{2}(n-1))}(E_{kin}-U_f^C)^{(3/2)n-5/2}$$

$$E_{kin} = E_{AZ}^* + m_0 c^2 - \sum_{i=1}^n m_i c^2$$
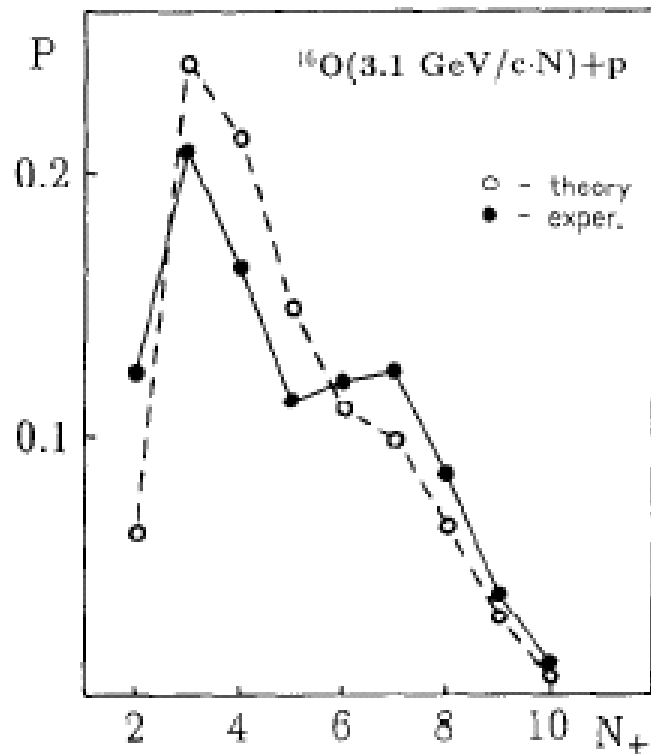
Fermi-break-up for
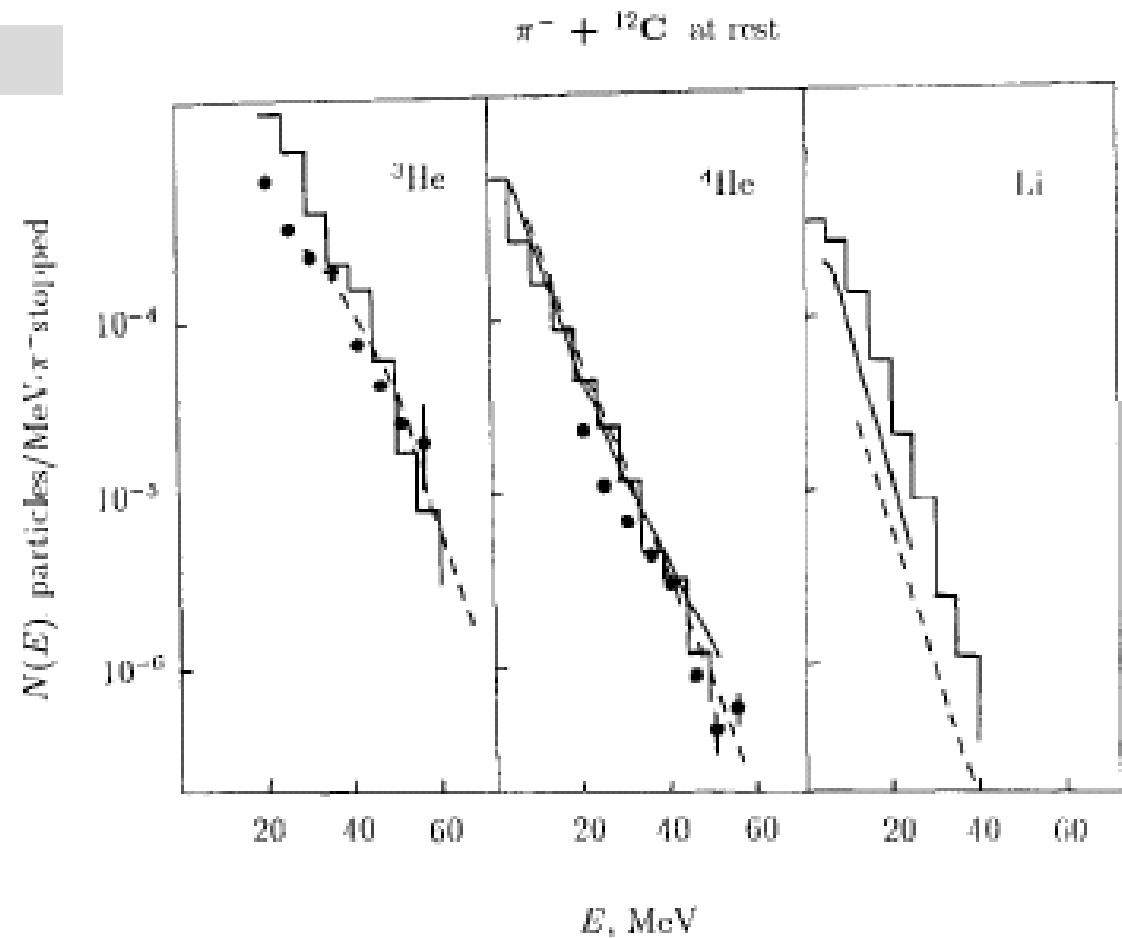light nuclei

$\pi^- + {}^{12}C$ at rest

Fig. 6.13. Energy spectra of He and Li fragments produced after absorption of stopped π^--mesons in ^{12}C nucleus. The detected particles are indicated in the figure. The histograms are calculated as described in the text. The experimental data: solid curves [160], dashed curves [161], dots [162].

Fig. 6.12. Multiplicity distribution of positively charged particles N_+ produced in $^{16}O(3.1$ GeV/c per nucleon) + p reaction. The dots are experimental data from [159]. The open circles are the CFEM calculation.
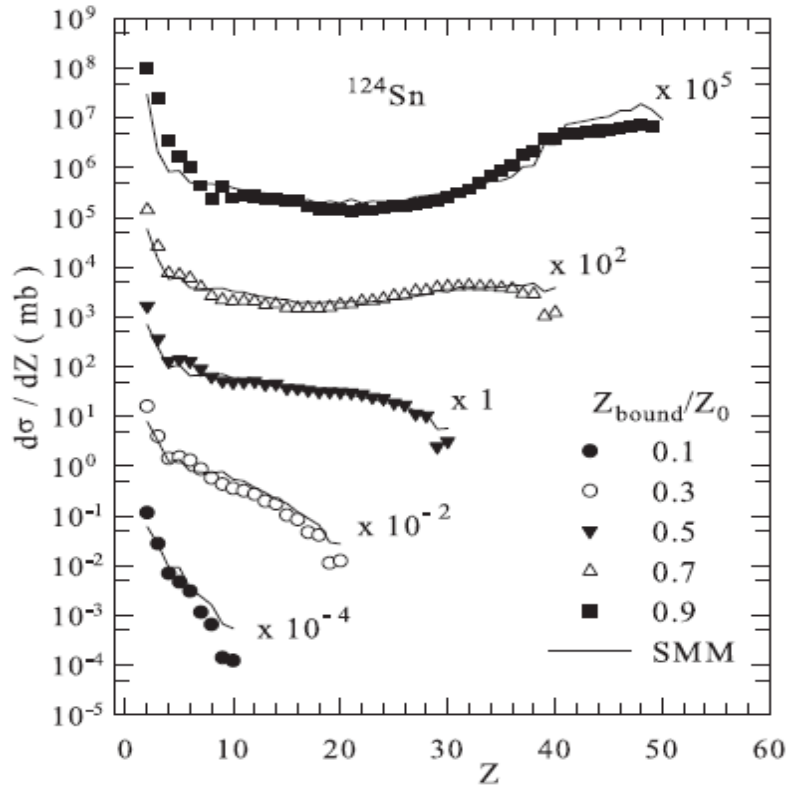
Isospin-dependent multifragmentation of relativistic projectiles

124,107-**Sn**, 124-**La** (600 A MeV) + **Sn** → projectile (multi-)fragmentation

Very good description is obtained within Statistical Multifragmentation Model, including fragment charge yields, isotope yileds, various fragment correlations.
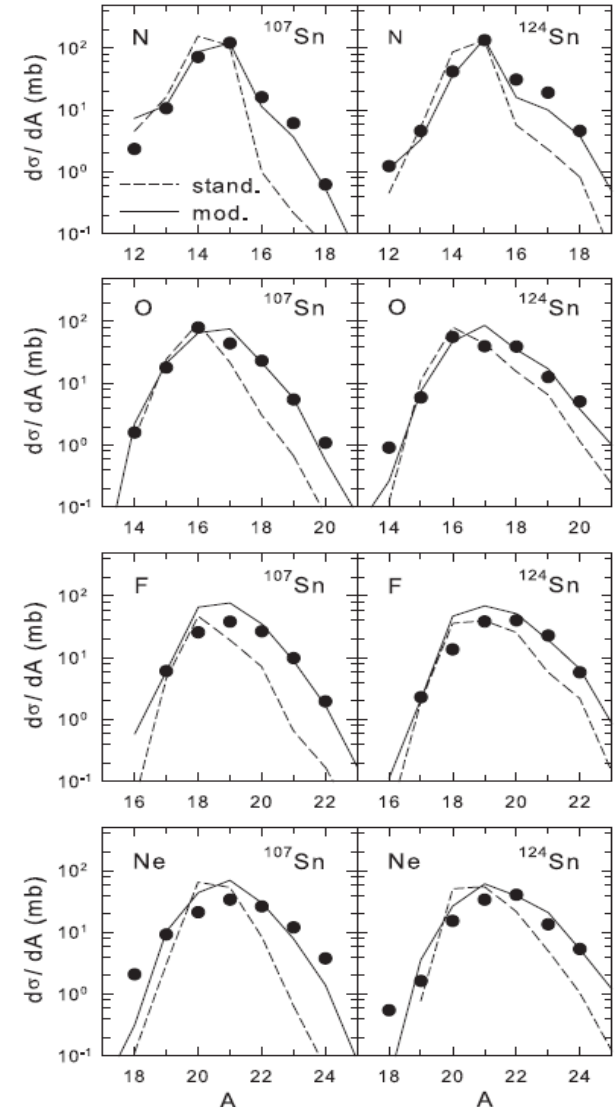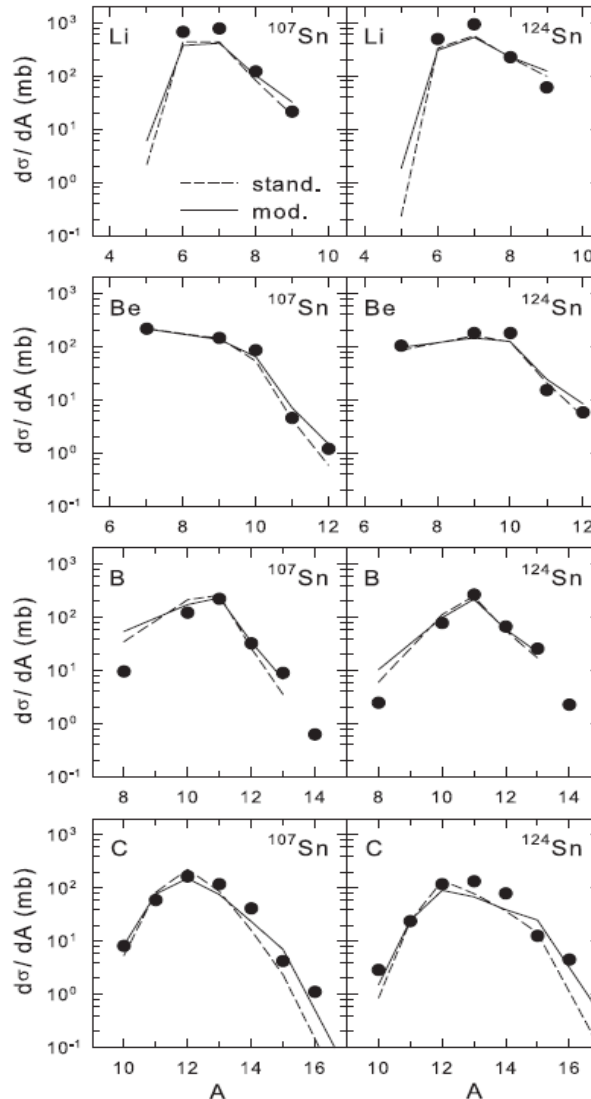
Statistical (chemical) equilibrium is established at break-up of hot projectile residues ! In the case of strangeness admixture we expect it too !

FRS data @ GSI

FRS projectile fragmentation of two symetric systems ^{124}Sn + ^{124}Sn and ^{112}Sn + ^{112}Sn at an incident beam energy of 1 A GeV measured with high-resolution magnetic spectrometer FRS.
(V. Föhr, et al., Phys. Rev. **C 84**, (2011) 054605)

Experimental data are well reproduced with statistical calculations in the SMM–ensemble .
To reproduce the FRS data symmetry energy term is reduced as shown in the table.
We have also found a decreasing trend of the symmetry energy with increasing charge number, for the neutron-rich heavy fragments resulting from ^{124}Sn projectile.
H. Imal, A.Ergun, N. Buyukcizmeci, R.Ogul, A.S. Botvina, W. Trautmann, C **91**, 034605 (2015)

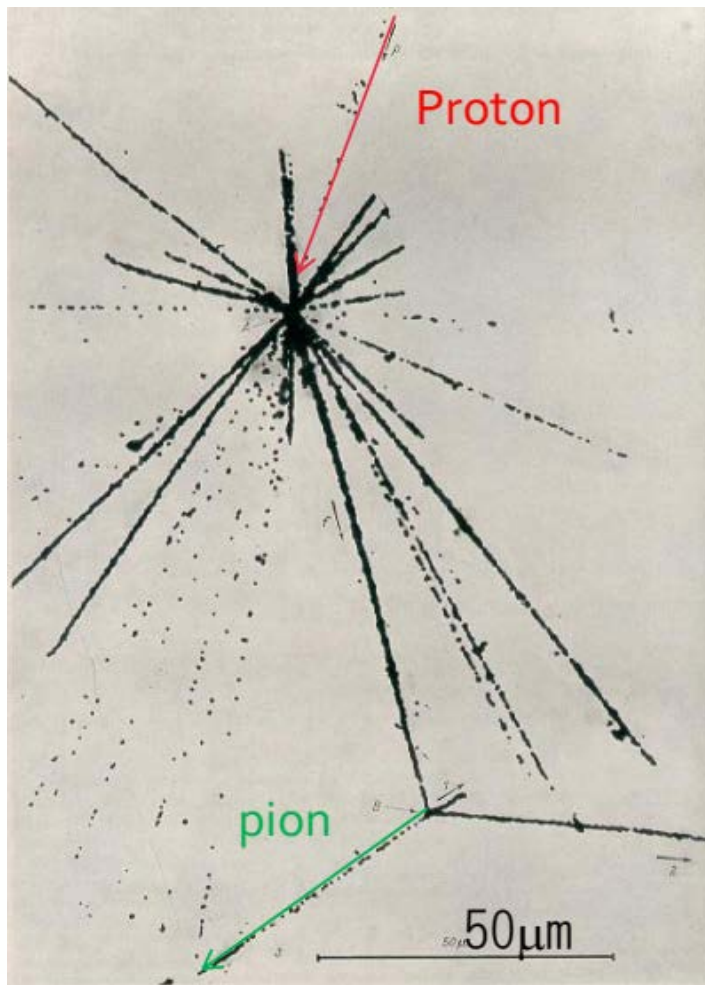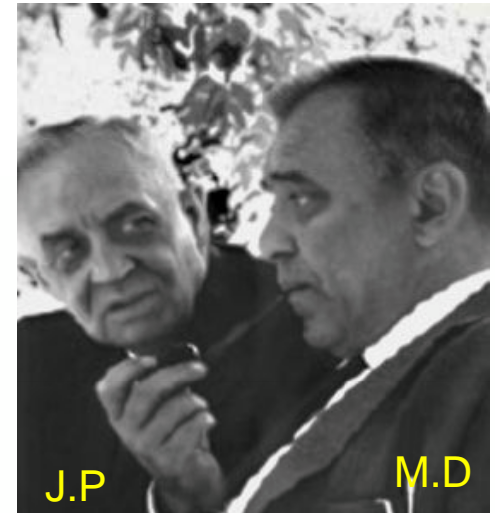Symmetry-energy coefficients.

Z interval	^{124}Sn γ(MeV)	^{112}Sn γ (MeV)
10-17	16	16
18-25	19	18
26-31	21	20
32-37	23	19
38-45	25	18
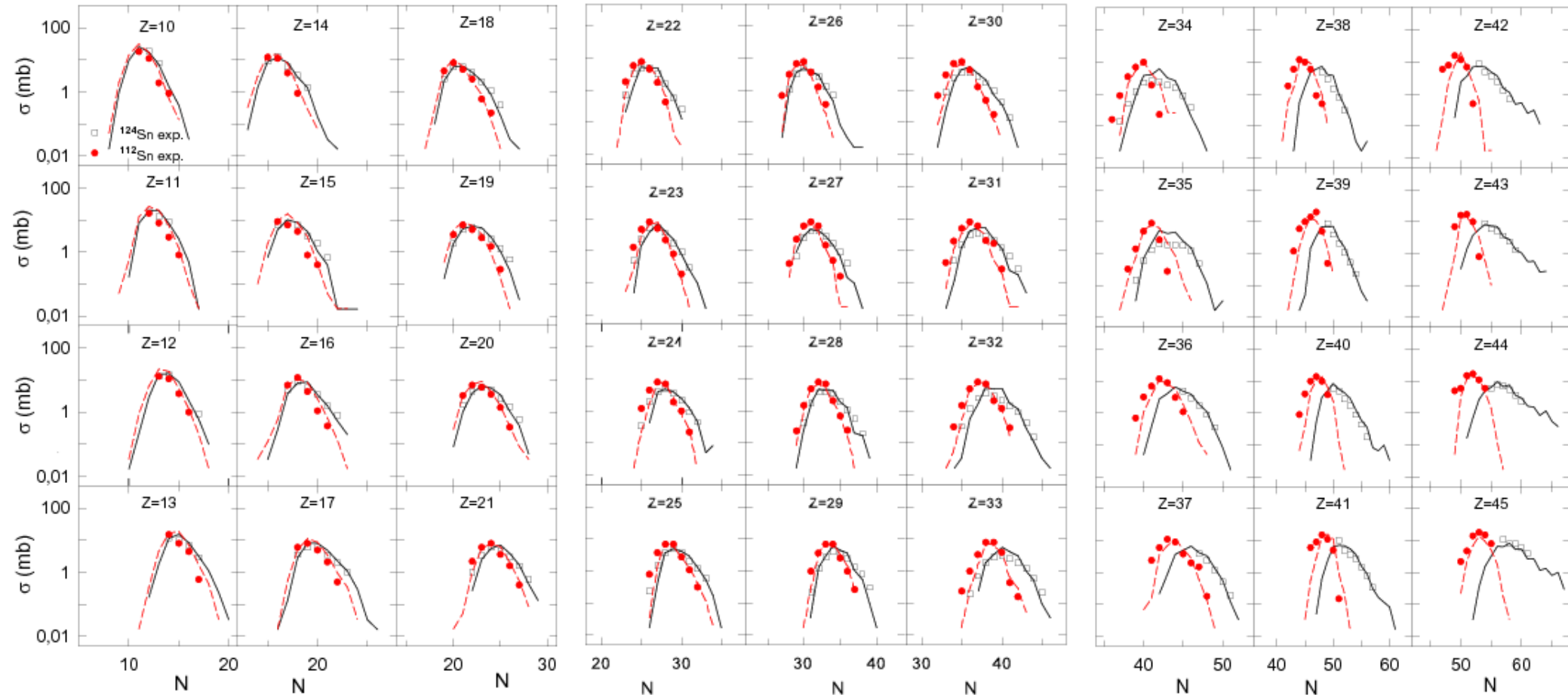
Discovery of a Strange nucleus: Hypernucleus

M. Danysz and J. Pniewski, Philos. Mag. 44 (1953) 348

First-hypernucleus was observed in a stack of photographic emulsions exposed to cosmic rays at about 26 k   above the ground.

J.P   M.D

Incoming high energy proton from cosmic ray

colliding with a nucleus of the emulsion, breaks it in several fragments forming a star.

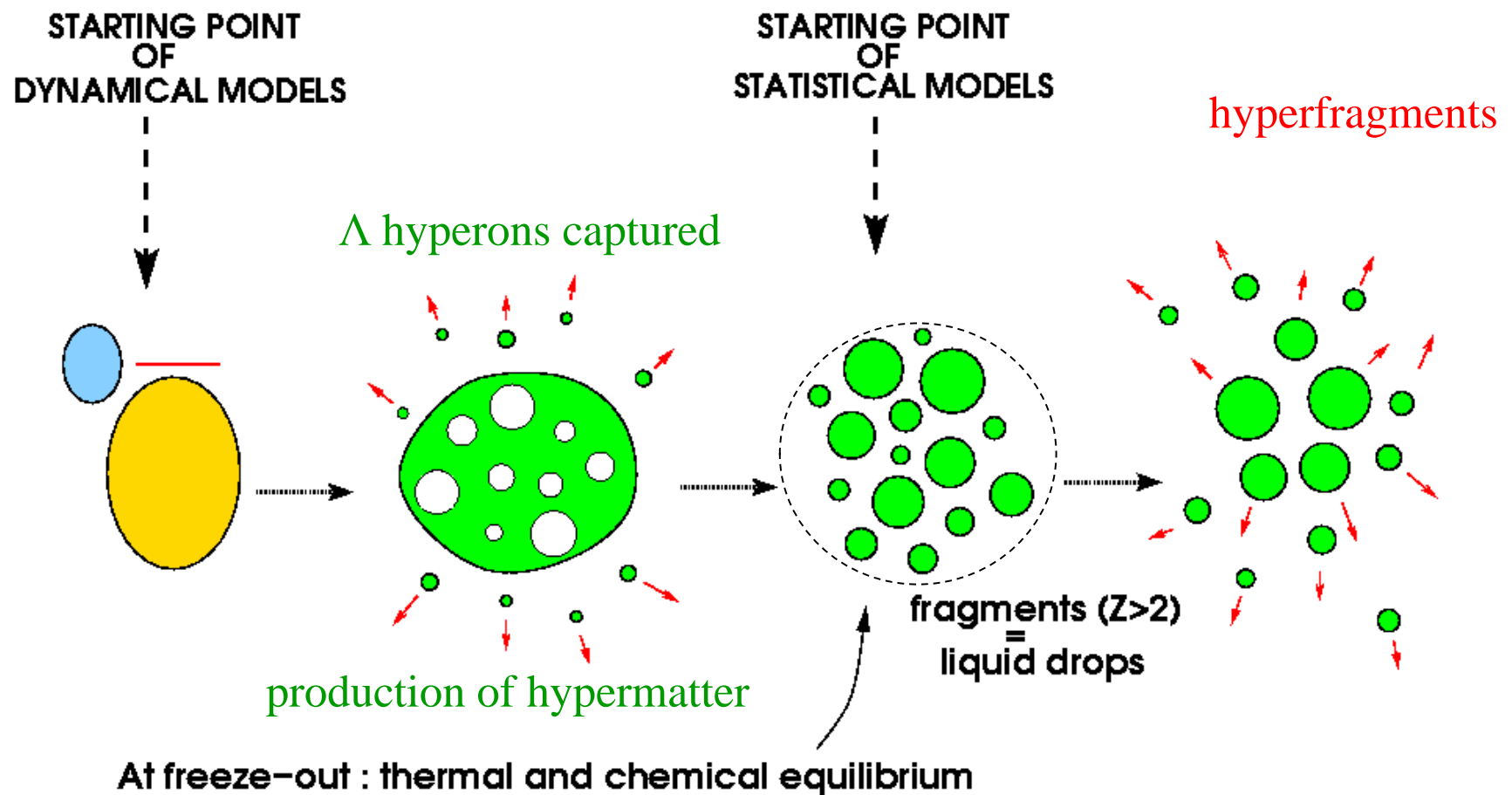All nuclear fragments stop in the emulsion after a short path

From the first star, 21 Tracks => 9α + 11H + 1 $_\Lambda$X

The fragment $_\Lambda$X disintegrates later , makes the bottom star. Time taken ~ 10^{-12} sec (typical for weak decay)

This particular nuclear fragment, and the others obtained afterwards in similar conditions, were called **hyperfragments or hypernuclei.**

Generalization of the statistical de-excitation model for nuclei with Lambda hyperons

In these reactions we expect analogy with

multifragmentation in intermediate and high energy nuclear reactions
+ nuclear matter with strangeness

STARTING POINT
OF
DYNAMICAL MODELS

STARTING POINT
OF
STATISTICAL MODELS

hyperfragments

Λ hyperons captured

production of hypermatter

fragments (Z>2)
=
liquid drops

At freeze−out : thermal and chemical equilibrium

Statistical approach for fragmentation of hyper-matter

$$Y_{AZH} = g_{AZH} V_f \frac{A^{3/2}}{\lambda_T^3} exp\left[-\frac{1}{T}(F_{AZH} - \mu_{AZH})\right]$$

mean yield of fragments with mass number **A**, charge **Z** ve **Λ** − hyperon number **H**

$$\mu_{AZH} = A\mu + Z\nu + H\xi$$

$$F_{AZH}(T,V) = F_A^B + F_A^S + F_{AZH}^{sym} + F_{AZ}^c + F_{AH}^{hyp}$$

Liquid-drop description of fragments: bulk, surface, symmetry, Coulomb (as in Wigner-Seitz approximation) and hyper energy contributions .

J. Bondorf et al. Phys. Rep. **257** (1995) 133.

$$F_A^B(T) = \left(-\omega_0 - \frac{T^2}{\varepsilon_0}\right)A$$

$$F_A^S(T) = \beta_0 \left(\frac{T_c^2 - T^2}{T_c^2 + T^2}\right)^{5/4} A^{3/2},$$

Bethe-Weizsacker formula parameters

$$\omega_0 = 16 \text{ MeV}, \beta_0 = 18 \text{ MeV}, T_c = 18 \text{ MeV}$$

$$F_{AZH}^{sym} = \gamma \frac{(A - H - 2Z)^2}{A - H}$$

$$\gamma = 25 \text{ MeV}, \varepsilon_0 \approx 16 \text{ MeV}$$

$$\sum_{AZH} AY_{AZH} = A_0, \sum_{AZH} ZY_{AZH} = Z_0, \sum_{AZH} HY_{AZH} = H_0$$

Chemical potentials are from mass, charge and hyperon number conservation μ, ν ve ξ

$$F_{AH}^{hyp} = E_{sam}^{hyp} = H \cdot \left[(-10.68 + 48.7)/A^{2/3}\right]$$

C. Samanta et al. J. Phys. G, **32** (2006) 363.

$$F_{AH}^{hyp} = (H/A) \cdot (-10.68A + 21.27A^{2/3}) \quad \rightarrow$$

Liquid-drop description of hyper-matter

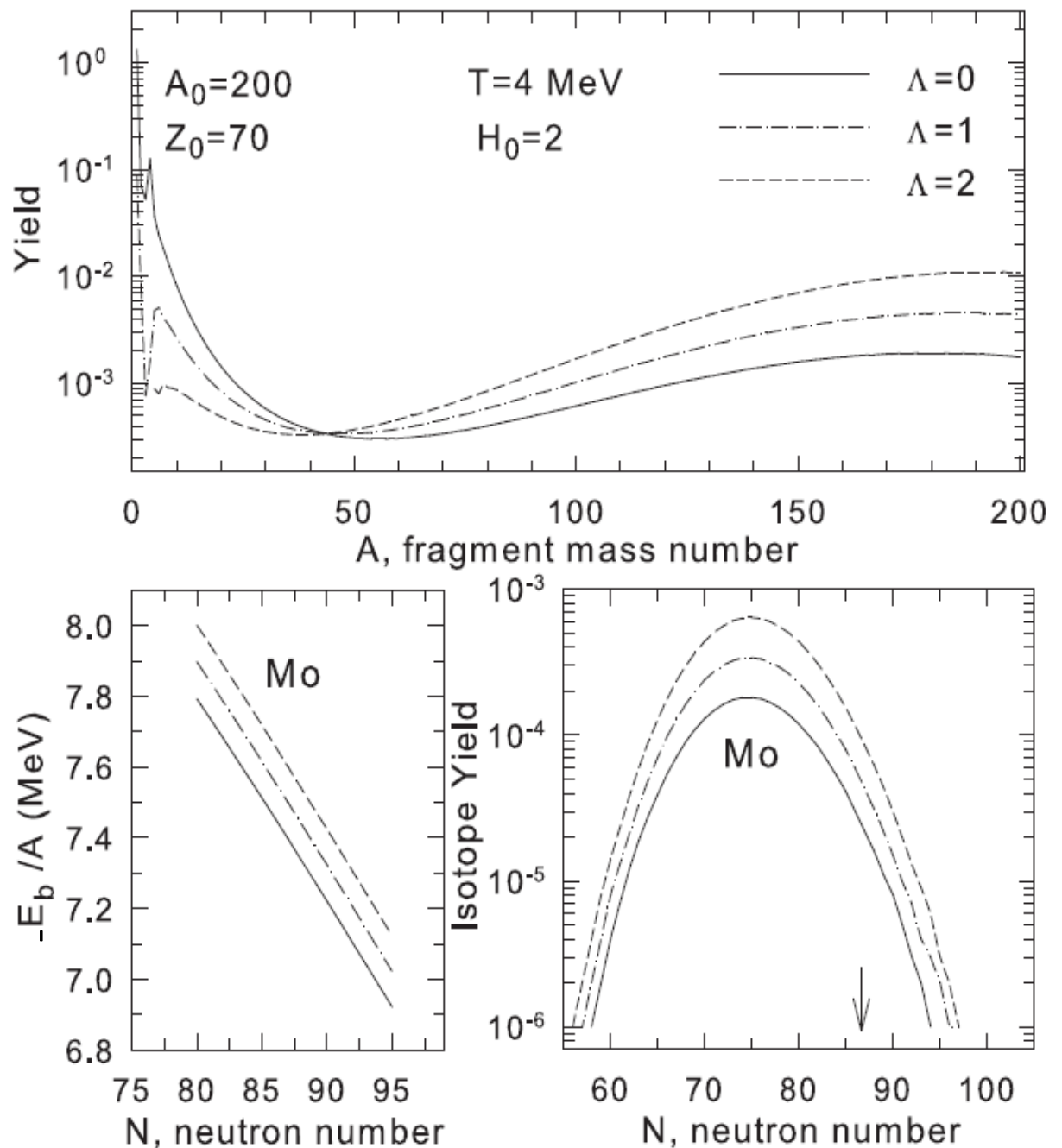A.S.Botvina and J.Pochodzalla, Phys. Rev.C76 (2007) 024909

Break-up of excited hyper-residues

Normal nuclei + hypernuclei can be formed via evaporation, fission and multifragmentation processes.

Liquid-gas type phase transition in hyper-matter is expected at subnuclear densities.

Very broad distributions of nuclei similar to ones in normal nuclear matter. At moderate temperatures hyperons concentrate in large species

Important: formed hypernuclei can reach beyond traditional neutron and proton drip-lines

N.Buyukcizmeci et al., PRC88 (2013) 014611

Fission of heavy hypernuclei formed in antiproton annihilation

Heavy hypernuclei are produced in the annihilation of antiprotons in ^{238}U. The delayed fission of heavy hypernuclei and hypernuclei of fission fragments are observed by using the recoil-distance method in combination with measurement of secondary electron multiplicity. The lifetime of hypernuclei in the region of uranium is found to be $(1.25 \pm 0.15) \times 10^{-10}$ sec. It is observed that Λ hyperons predominantly stick to the heavier fission fragments. The yield of hypernuclei is found to be $(7.4 \pm 1.7) \times 10^{-3}$ per stopped antiproton. No coincidences with K^+ were found. Statistical and systematic errors on the number of events expected do not rule out this possibility.

The main results of the present experiment are the following. (i) The annihilation of antiprotons in ^{238}U leads to the production of hypernuclei of fission fragments and of heavy hypernuclei in the region of uranium. (ii) The lifetime of the heavy hypernuclei is found to be $(1.25 \pm 0.15) \times 10^{-10}$ sec. (iii) When the fission of an excited hypernucleus occurs, the Λ hyperon predominantly sticks to the heavy fragment; this fact can be used in the analysis of the dynamics of fission [17]. (iv) The probability of Λ-hyperon attachment to a heavy nucleus, following $\bar{p}$ annihilation, is estimated to be about 25%. (v) We do not find with significant confidence that K^+ are produced in coincidence with the hypernuclear events. However, this conclusion depends on complex and poorly known features of kaon production in heavy nuclei.
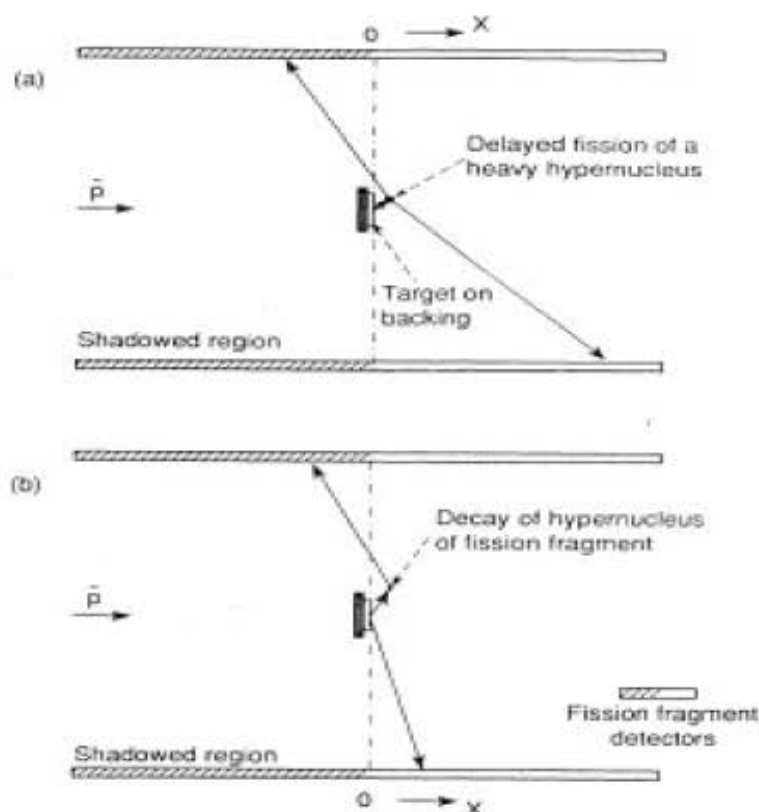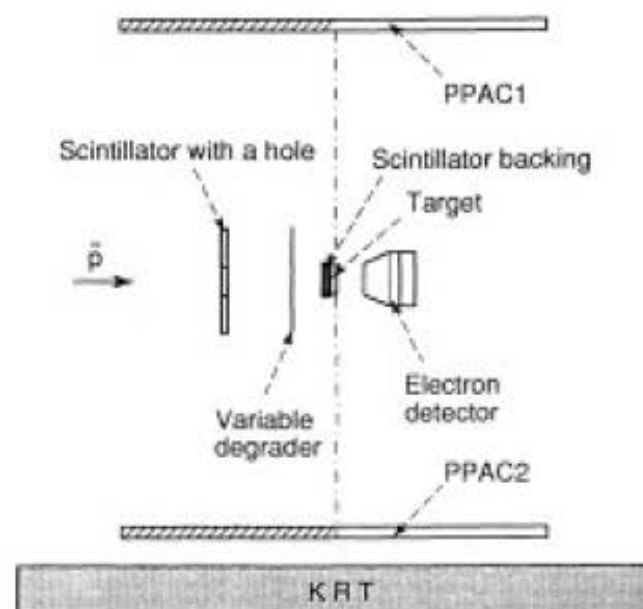

FIG. 1. Schematic representation of the recoil-distance method as applied to the study of (a) delayed fission of heavy hypernuclei, and (b) decay of hypernuclei of fission fragments. Both types of events can provide hits in the shadowed region (hatched) of the detectors while prompt fission cannot.

FIG. 2. Scheme of the experimental setup (not to scale). PPAC is the parallel plate avalanche counter; KRT is the Kaon range telescope.

Λ-hyperon lifetime in very heavy hypernuclei produced in the $p+U$ interaction

The recoil shadow method for the detection of fission fragments has been used to investigate delayed fission of very heavy Λ hypernuclei produced in the p-U interaction at the projectile energy of 1.5 GeV. From the measured distribution of delayed fission events in the shadow region and the calculated momenta of hypernuclei leaving the target the lifetime of the Λ hyperon in very heavy hypernuclei was determined to be $\tau = 2.40 \pm 60$ ps. The comparison of the number of delayed fission events with that of the prompt events leads to an estimation of the cross section for the production of Λ hypernuclei in $p+U$ collisions at 1.5 GeV of $\sigma_{Hv} = 150^{+150}_{-80}$ μb. [S0556-2813(97)04506-8]

H. Ohm et al., PRC 55 (1997) 3062
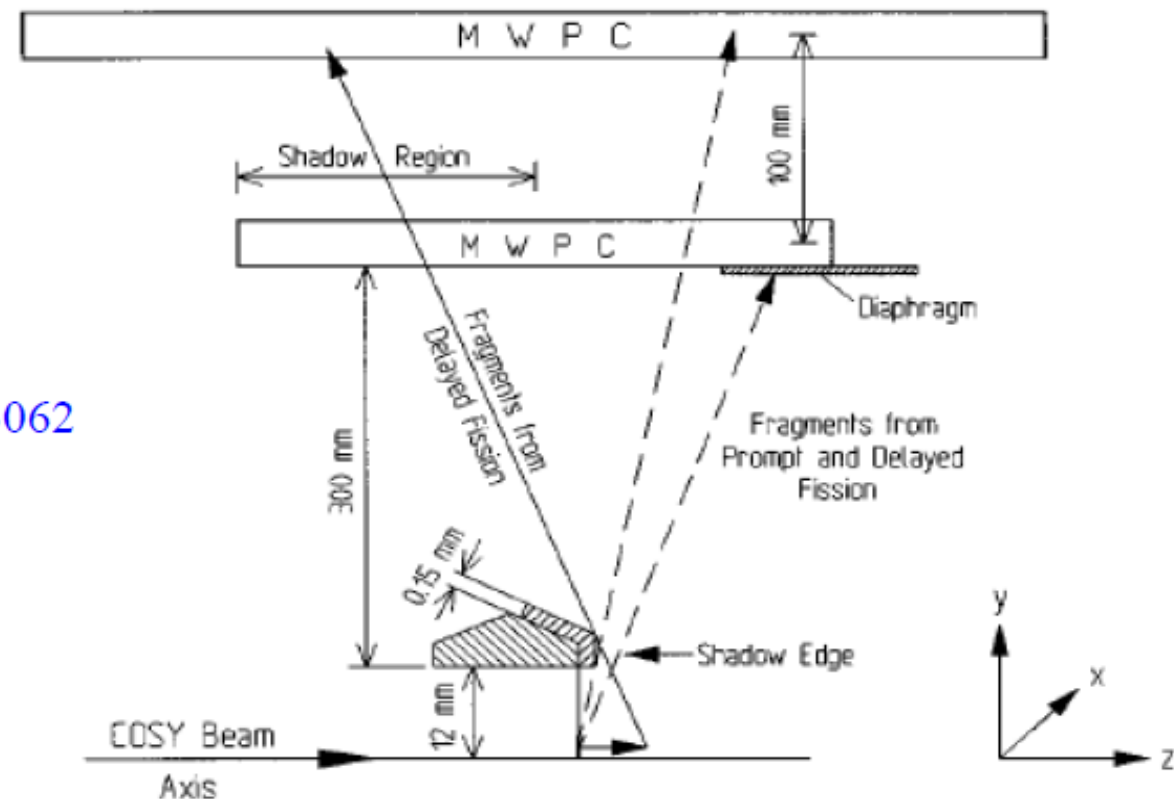
FIG. 1. Schematic presentation of the experimental setup. The thickness of the target holder is enhanced in the drawing to show the details. The real distances are given.
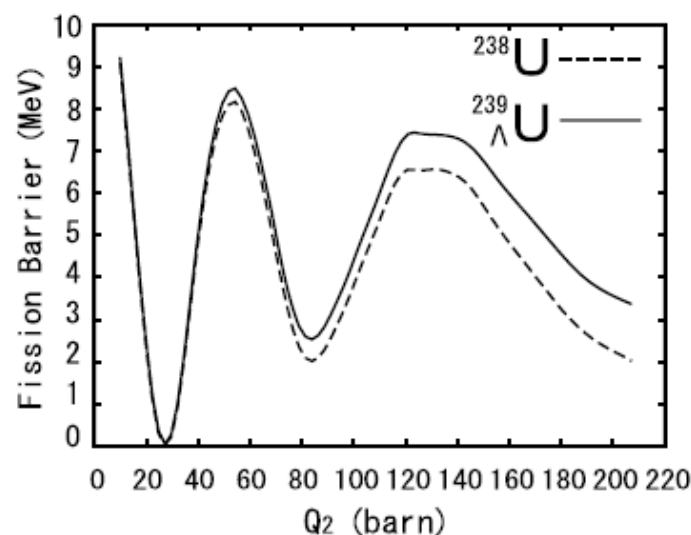
Table 1
The height of the inner and outer fission barriers for the ^{238}U and $^{239}_{\Lambda}$U nuclei when the Λ particle occupies the lowest single-particle state during fission.

	^{238}U	$^{239}_{\Lambda}$U
B_f (inner) (MeV)	8.20	8.47
B_f (outer) (MeV)	6.60	7.42

Fig. 1. The fission barrier of ^{238}U (the dotted line) and $^{239}_{\Lambda}$U (the solid line) nuclei obtained with the Skyrme–Hartree–Fock method. The Λ particle is assumed to occupy the lowest single-particle state during fission. The energy curves are shifted so that the ground state configuration has zero energy.
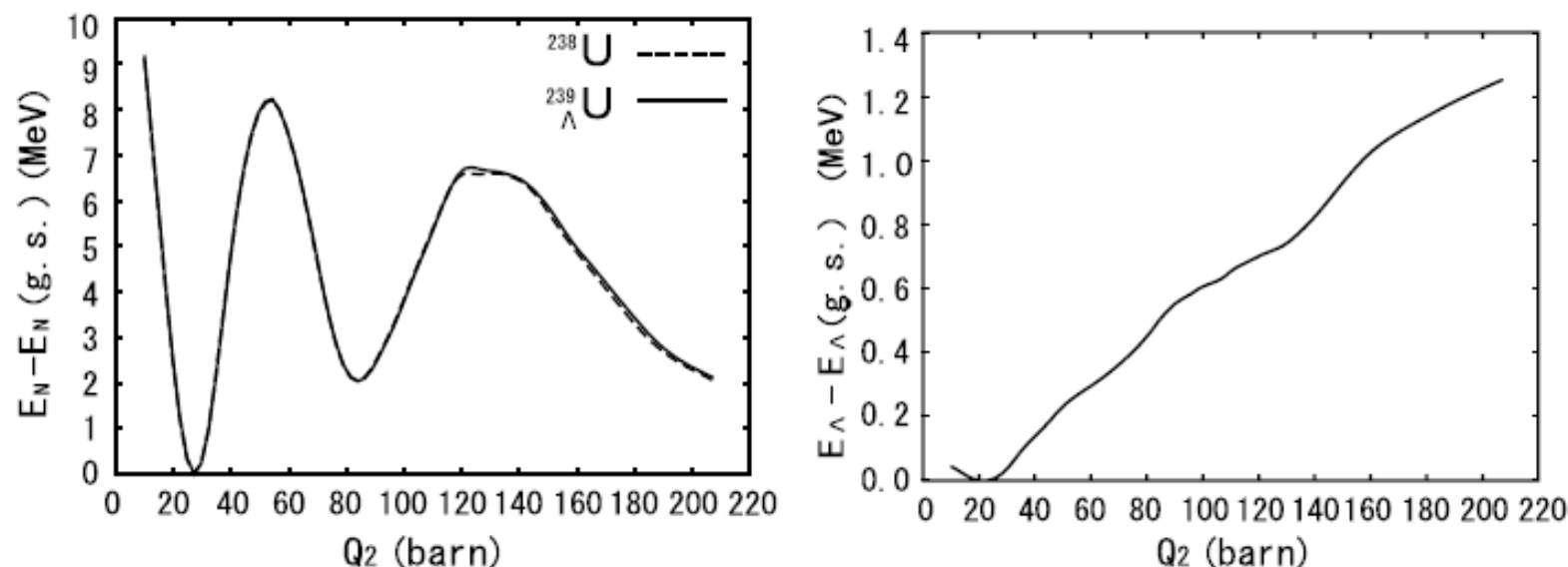
Fig. 2. (The left panel): The energy of the core nucleus E_N for the ^{238}U (the solid line) and $^{239}_{\Lambda}$U (the dashed line) nuclei as a function of the total quadrupole moment Q_2. The Λ particle is assumed to be at the lowest single-particle state. (The right panel): The energy of the Λ particle E_Λ for $^{239}_{\Lambda}$U with respect to that for the ground state as a function of Q_2.

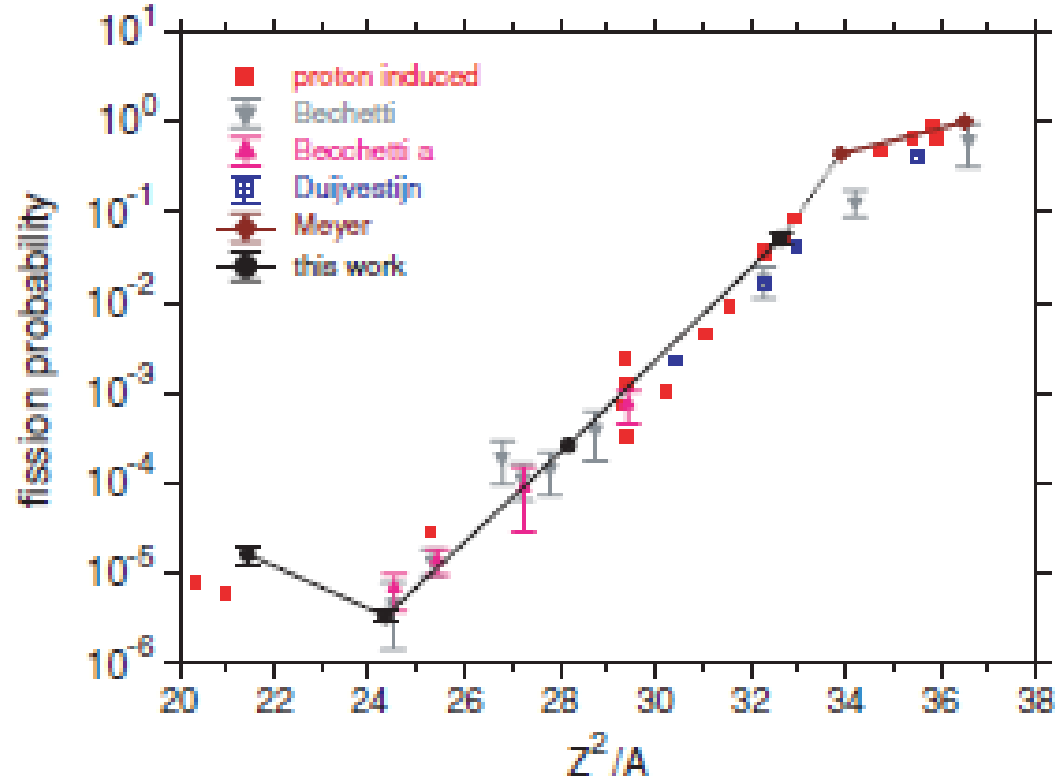# Fission studies with 140 MeV α particles

FIG. 4. (Color online) The fission probability as a function of the fissility parameter. The dots with error bars are the present results and diamonds are from Ref. [21]. The lines are to guide the eye. The squares are for proton-induced fission at energies 150 to 200 MeV [22,23]. The other data shown were measured with 190 MeV protons: triangles down [24], triangles up [25], and those shown by crossed squares were measured by radiochemical methods [26].

TABLE II. Cross section for fission for the different target nuclei. Also given are estimates for the fission barriers obtained by the linear dependence of the fission parameter [denoted by (I)] and on the exponential given in the text [denoted by (II)].

Target	σ_{fiss} (mb)	B_f (MeV) (I)	B_f (MeV) (II)
^{nat}Ag	0.030 ± 0.007	38.8	49.1
^{139}La	0.007 ± 0.001	49.5	62.8
^{165}Ho	0.600 ± 0.050	40.8	45.4
^{197}Au	128 ± 18	26.9	25.7

Statistical calculations of probabilities of the heavy hyper-nuclei's fission and evaporation of Lambda-hyperons.
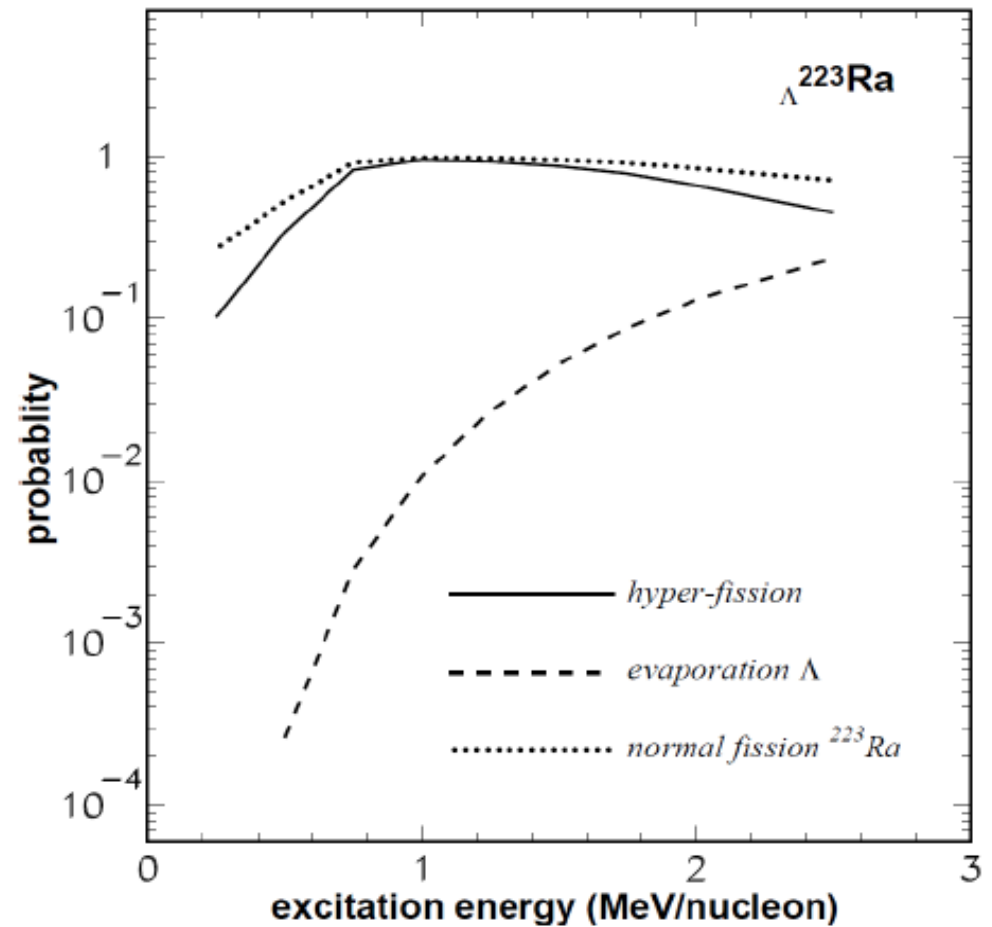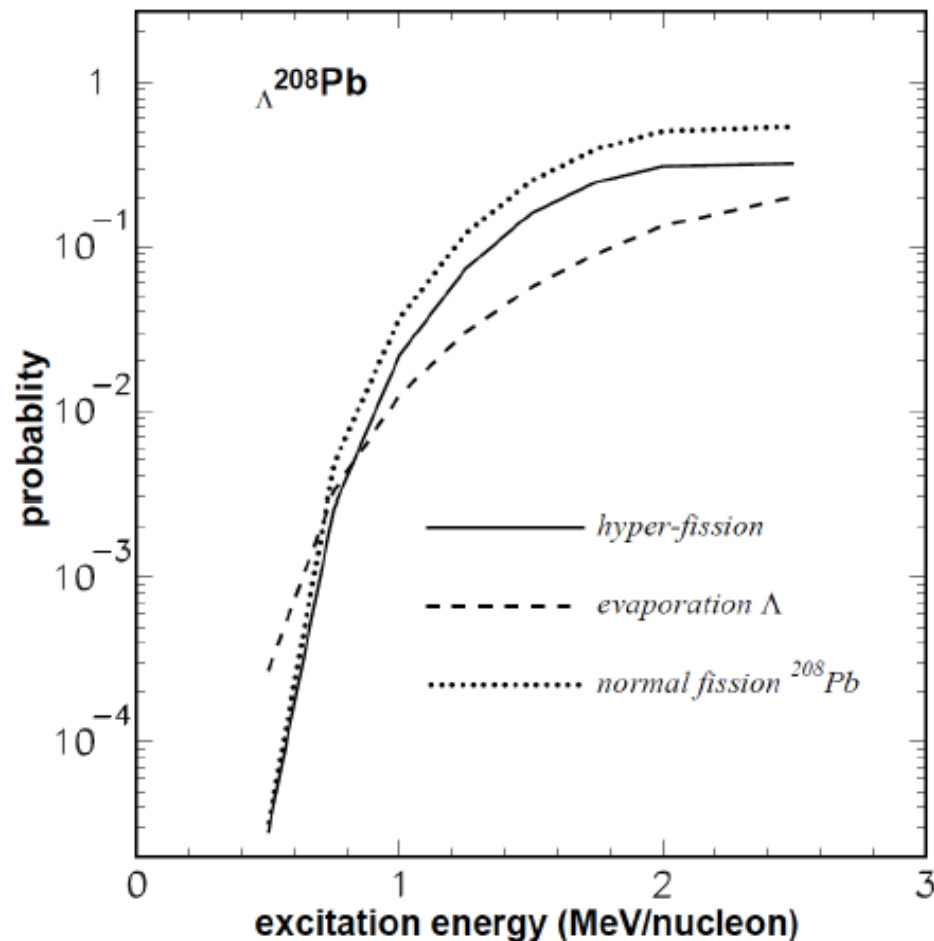

Estimated hyper-fission cross-section taking into account the dynamical stage for p(2GeV)+U :

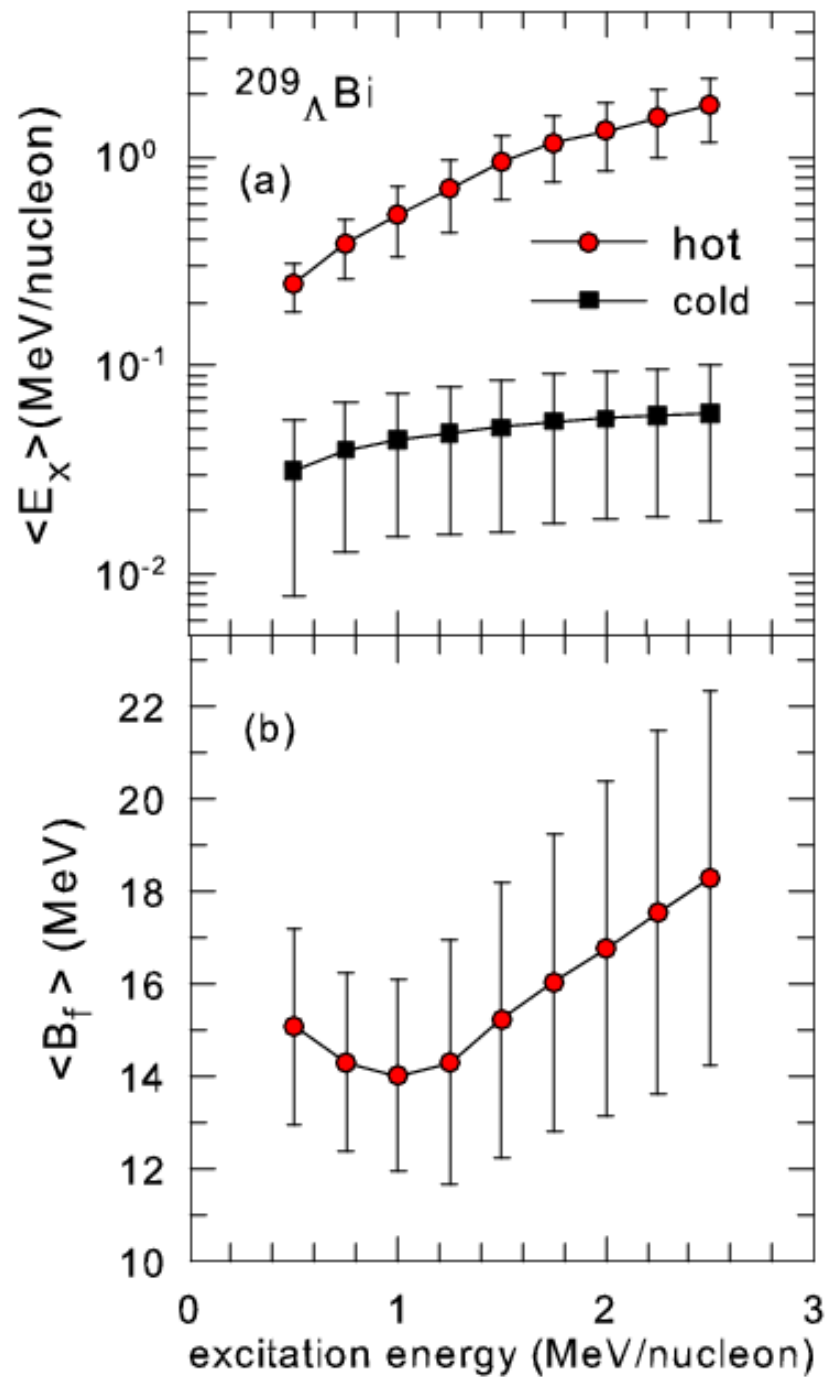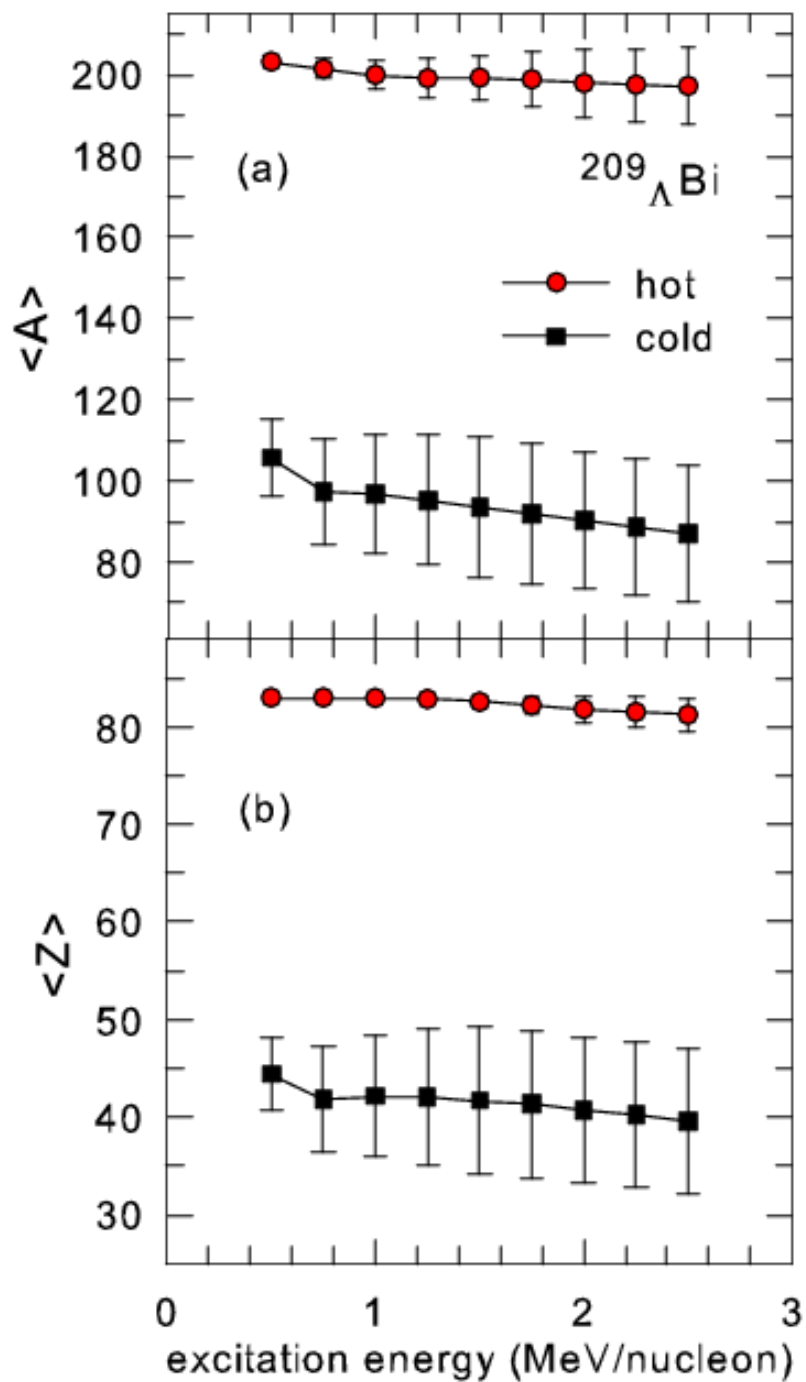Sigma ~ 2000 mb * 0.001 * 0.5 ~ 1 mb

It is practically as the fission cross-section in normal muclei (i.e., for U ~ 1 b , Pb ~ 200 mb …) by high energy protons, scaled by the factor of the hyperon capture. In addition, there is a delayed fission caused by the Lambda-hyperon decay in the hyper-nucleus.
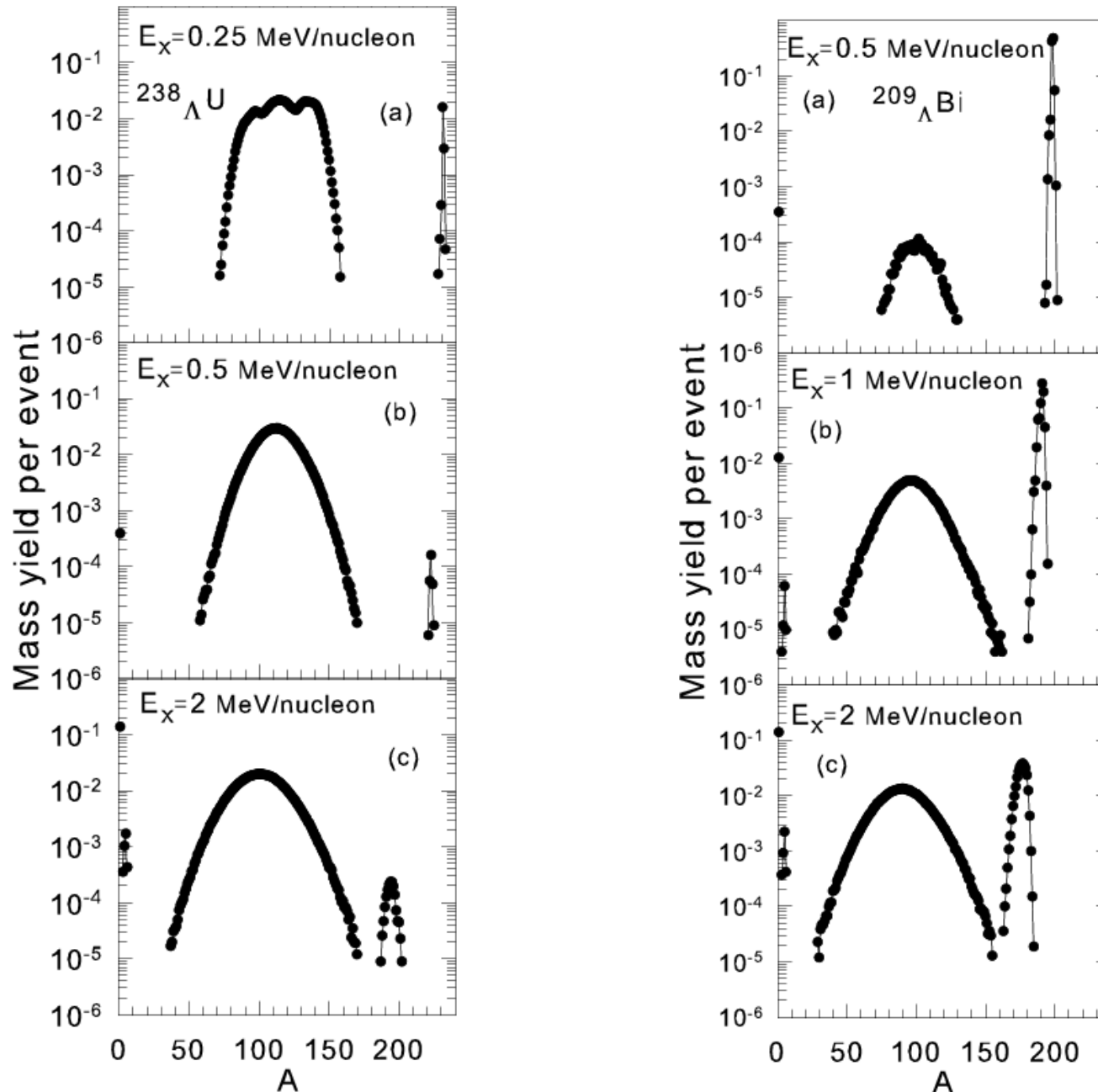
normal   hyper
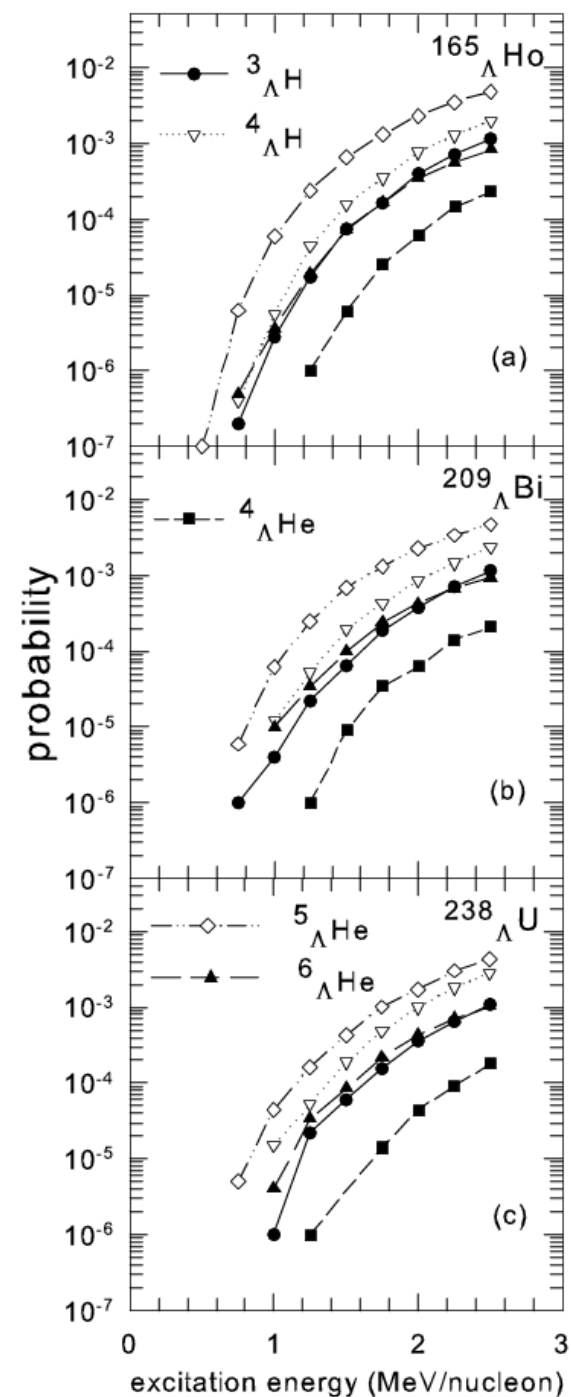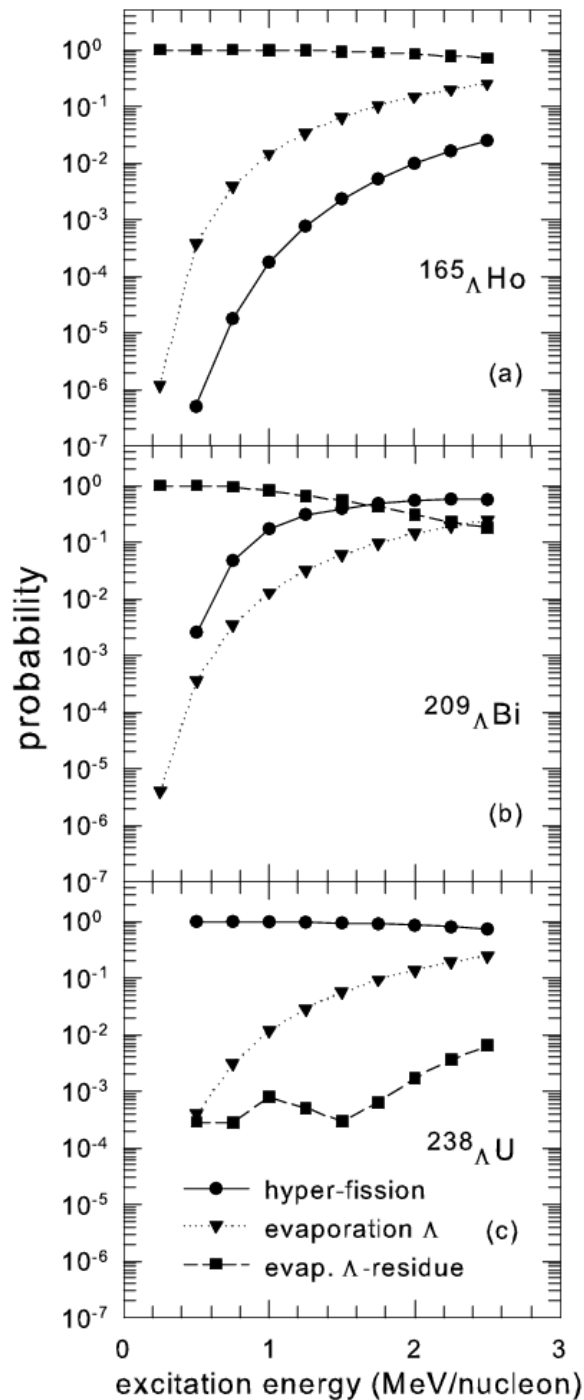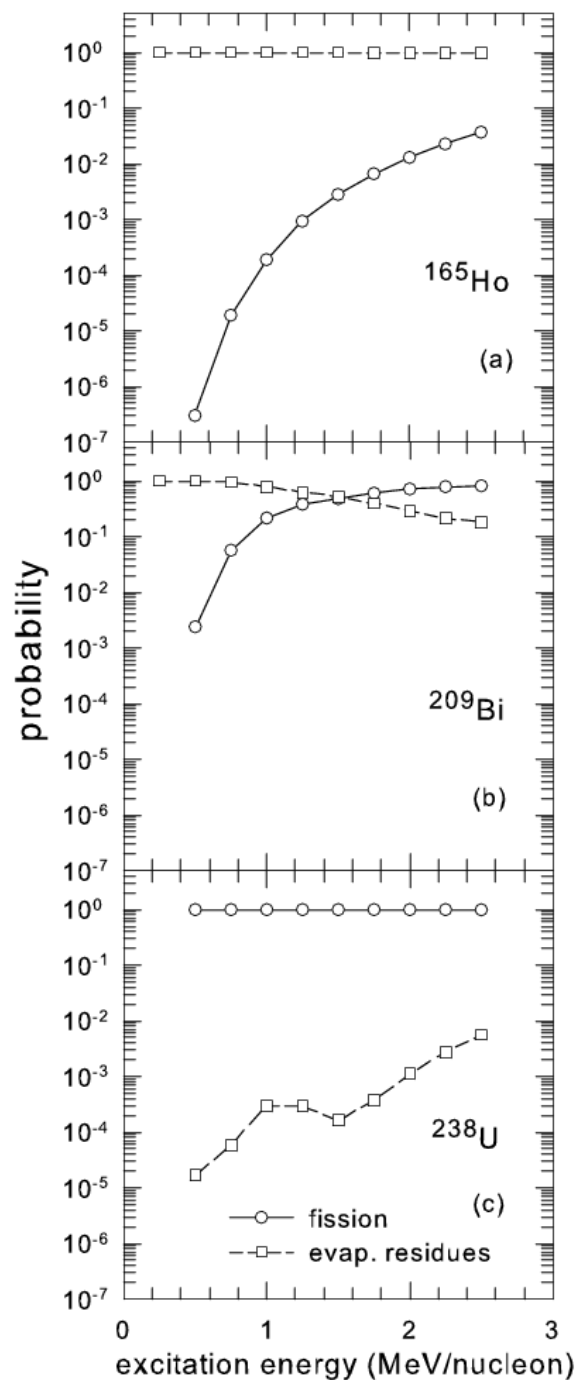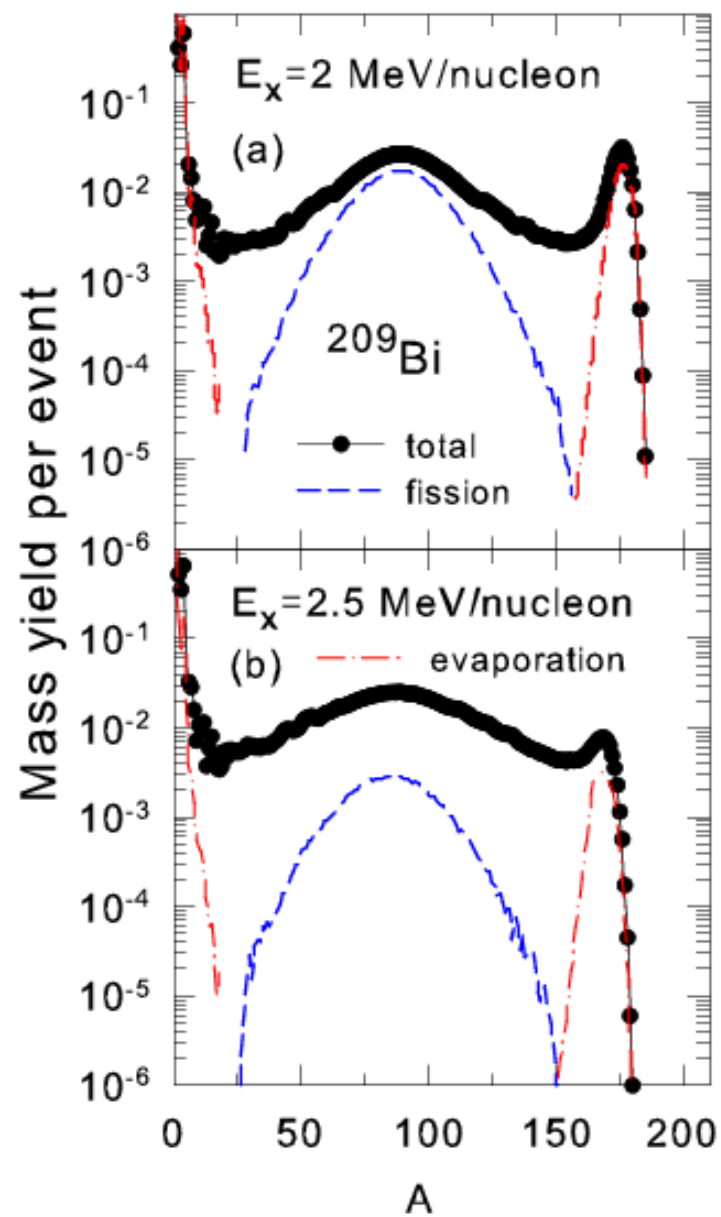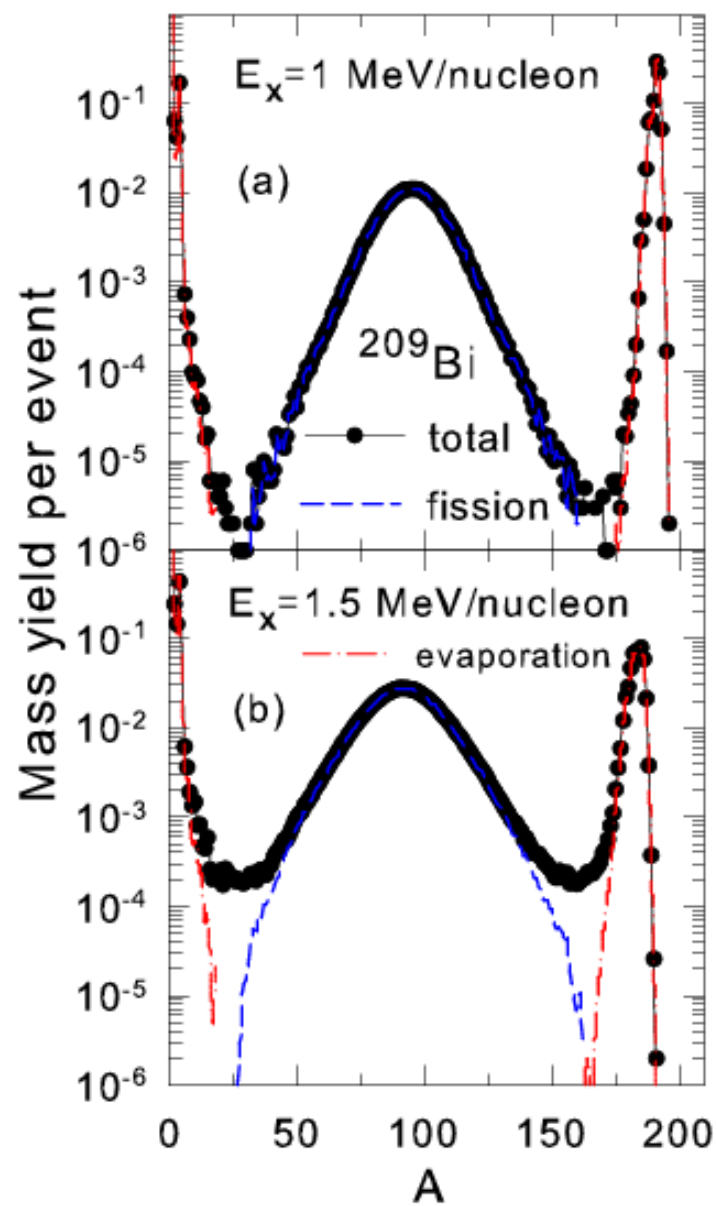
Hyper fragment distributions (Λ=1) for different excitation energy

Botvina et al. PhysRevC 94 054615 (2016)

$N_u \sim N_d \sim N_s$

$S = -\infty$

Strangeness in neutron stars ($\rho > 3 - 4\,\rho_0$)

Strange hadronic matter ($A \to \infty$)

$p, n, \Lambda, \Xi^0, \Xi^-$

higher density

$\Lambda\Lambda$, Ξ hypernuclei

ΛN interaction

$S = -2$

Λ, Σ hypernuclei

Proton-rich nuclei

Λ

$S = -1$

Neutron-rich nuclei

Strangeness

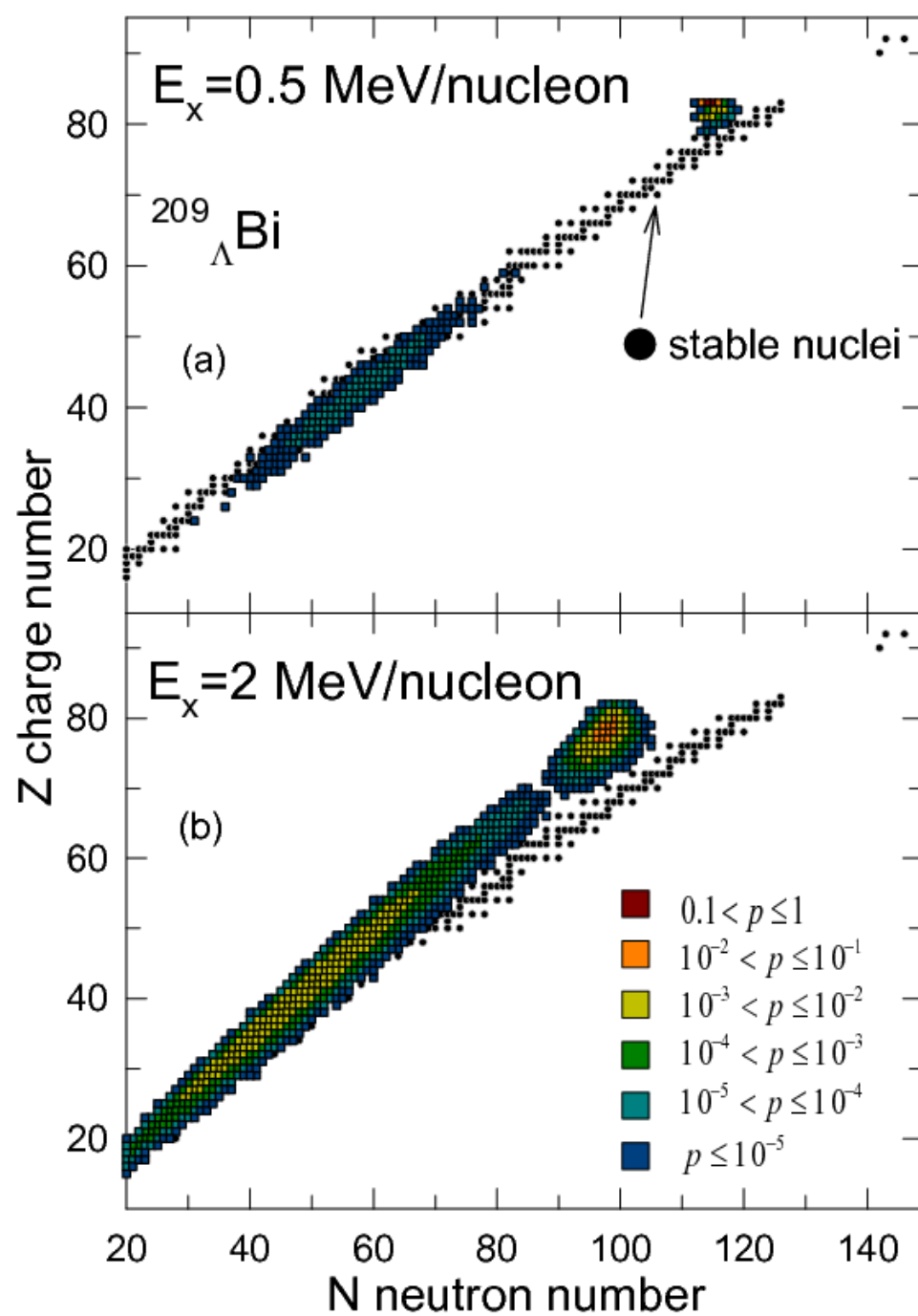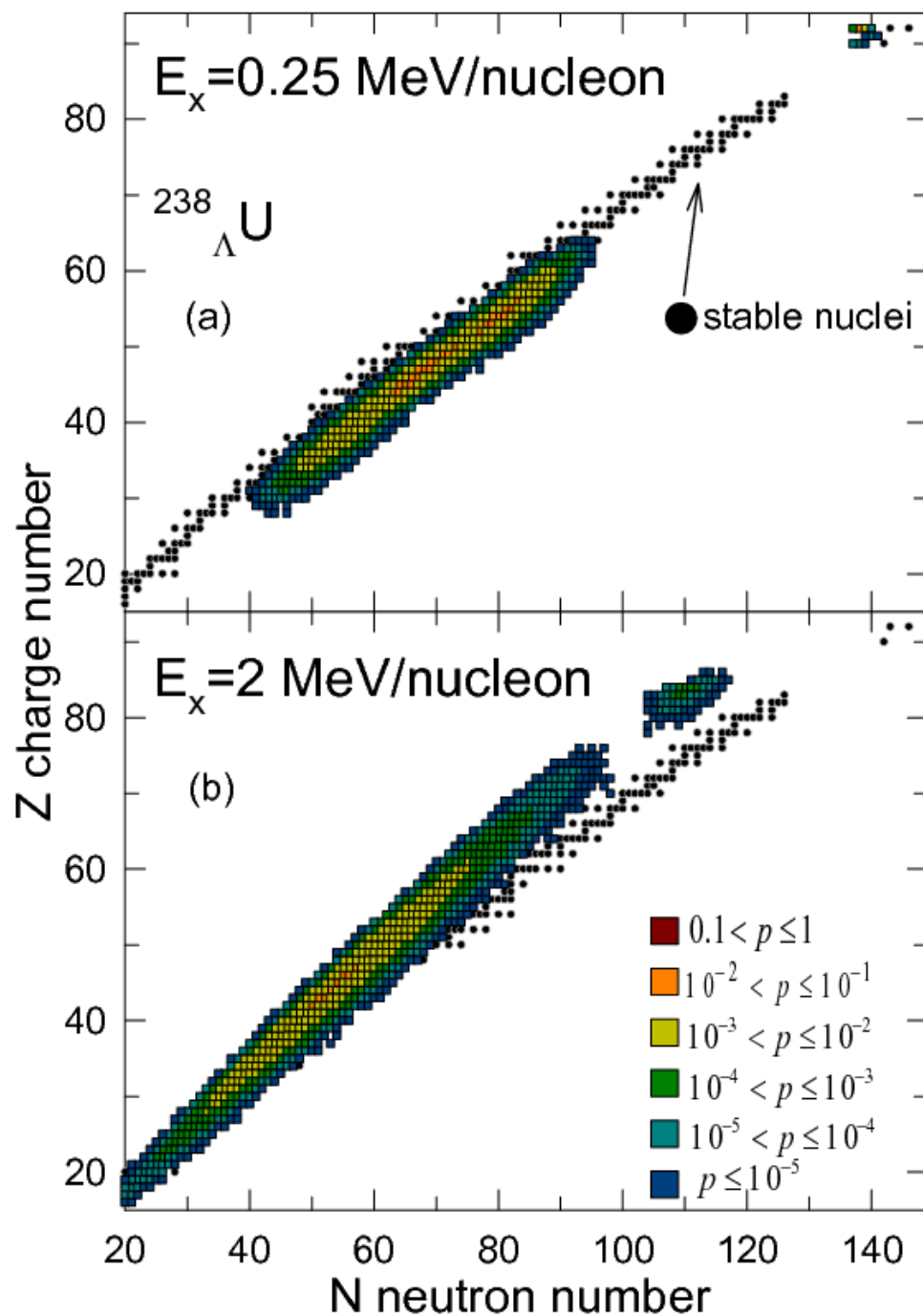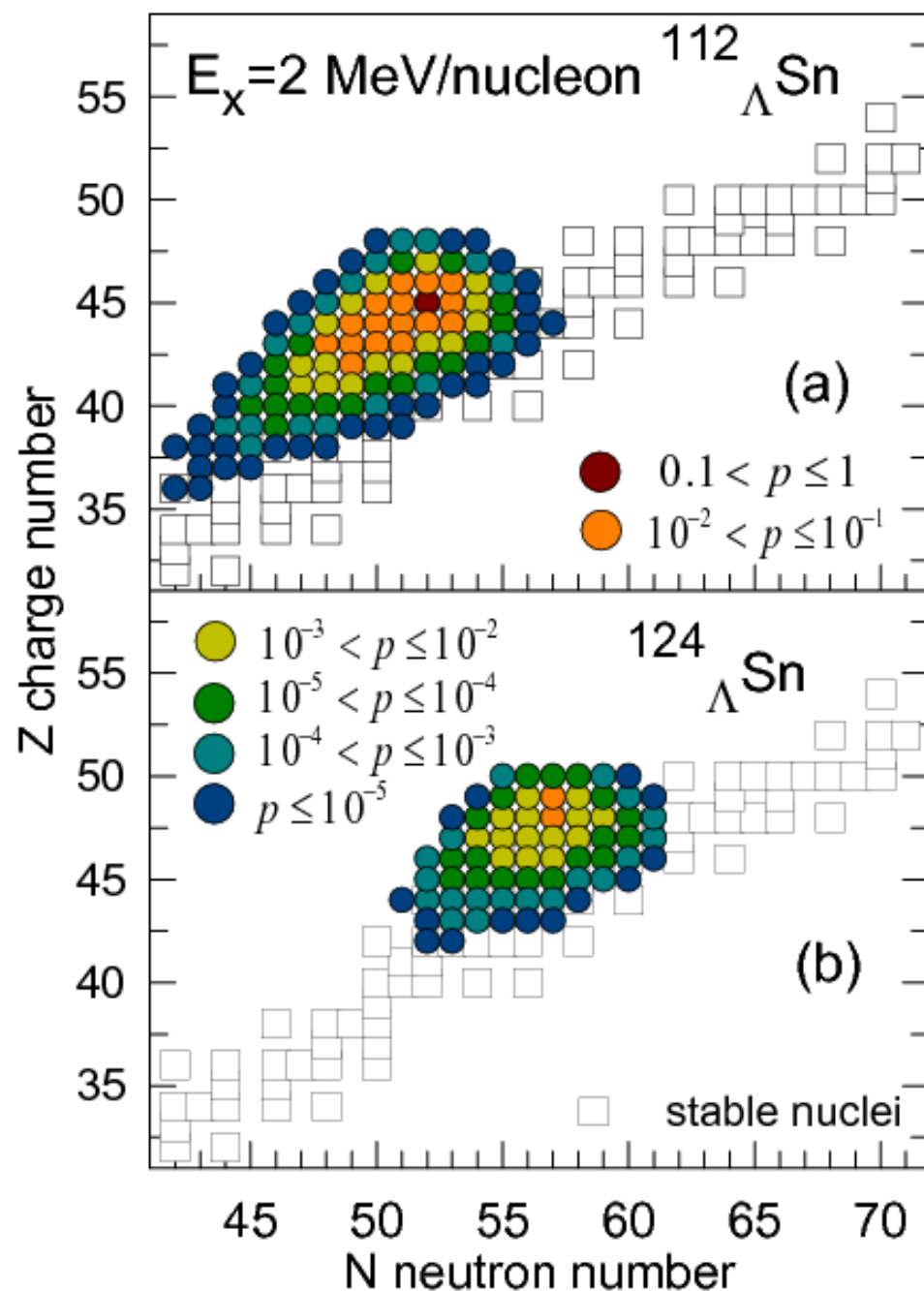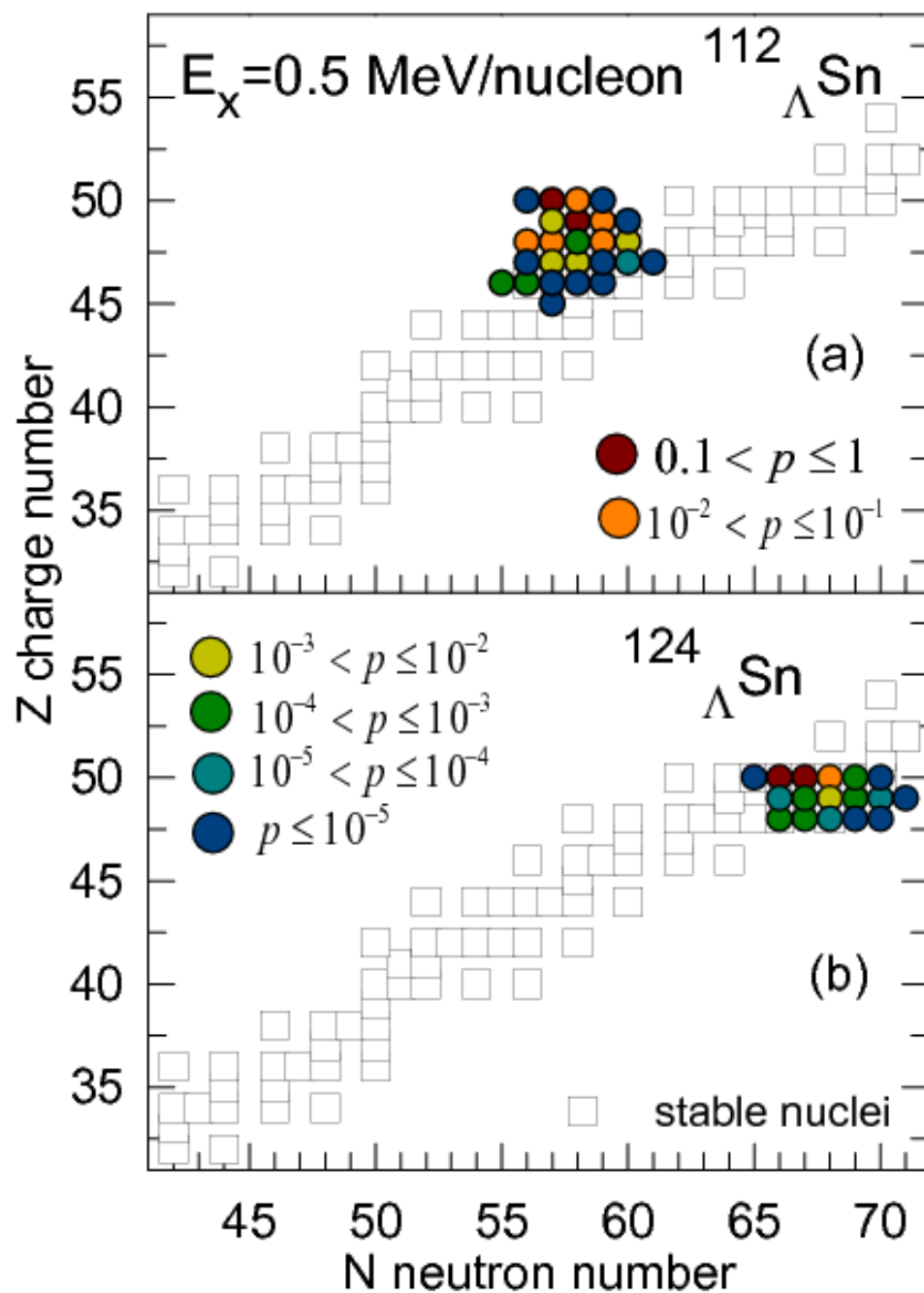proton number

non-strange nuclei

neutron halo

p   n

neutron number

3-dimensional nuclear chart

Nuclear chart for stellar matter
Statictical Model for Supernova Matter (SMSM) calculations
N. Buyukcizmeci, collaboration with A.S. Botvina and I.N. Mishustin (2016)

In future, we plan to include hypernuclei in these kind of calculations for supernova matter.
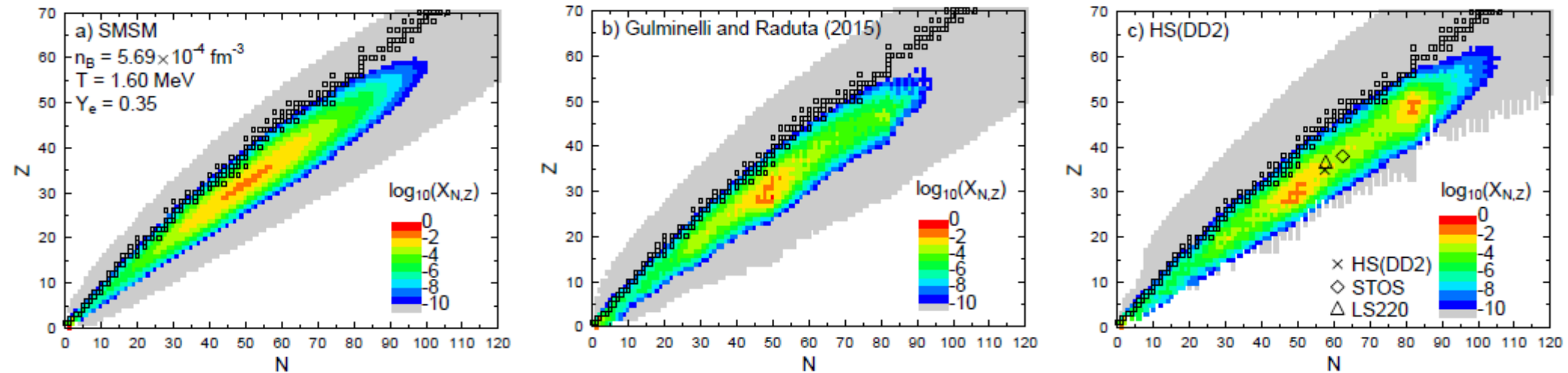

FIG. 10 Composition of matter in the center of a CCSN 6 ms before bounce at thermodynamic conditions taken from a simulation of Perego et al. (2015). The color map shows the distribution of nuclei (mass fractions) in the SMSM (Buyukcizmeci et al., 2014) (a), the EoS of Gulminelli and Raduta (2015) (b) and the HS(DD2) model (c). The black cross indicates in panel (c) the average heavy nucleus. The black diamond and triangle show the representative heavy nucleus of STOS and LS220, respectively, calculated within the SNA. (color online)

M. Oertel, M. Hempel, T. Klahn, S. Typel , Rev. Mod. Phys. 89, 015007 (2017)

Double ratio method for hypernuclei

Grand canonical approximations leads to the following average yields of individual fragments with the mass (baryon) number A, charge Z and the Λ-hyperon number H:

$$Y_{AZH} = g_{AZH} V_f \frac{A^{3/2}}{\lambda_T^3} exp\left[-\frac{1}{T}(F_{AZH} - \mu_{AZH})\right] \qquad F_{AZH}(T,V) = F_A^B + F_A^S + F_{AZH}^{sym} + F_{AZ}^C + F_{AH}^{hyp}$$

$$\mu_{AZH} = A\mu + Z\nu + H\xi \qquad\qquad F_{AH}^{hyp} = (H/A)\cdot(-10.68A + 21.27A^{2/3})$$

It is convenient to rewrite the above formulas in order to show separately the binding energy E_A^{bh} of one hyperon at the temperature T inside a hypernucleus with A, Z, H:

$$E_A^{bh} = F_{A,Z,H} - F_{A-1,Z,H-1} \ . \qquad (4)$$

Since Λ-hyperon is usually bound, this value is negative. Then the yield of hypernuclei with an additional Λ hyperon can be recursively written by using the former yields:

$$Y_{A,Z,H} = Y_{A-1,Z,H-1} \cdot C_{A,Z,H} \cdot exp\left[-\frac{1}{T}\left(E_A^{bh} - \mu - \xi\right)\right], \qquad (5)$$

where $C_{A,Z,H} = (g_{A,Z,H}/g_{A-1,Z,H-1}) \cdot (A^{3/2}/(A-1)^{3/2})$ depends mainly on the ratio of the spin factors of A, Z, H and $A-1, Z, H-1$ nuclei, and very weakly (especially for large nuclei) on A. Since in the liquid-drop approximation we assume that the fragments with $A > 4$ are excited and do populate many states (above the ground) according to the given temperature dependence of the free energy, then we take $g_{A,Z,H} = 1$. Within SMM

We suggest the following receipt for obtaining information on the binding energies of hyperons inside nuclei. Let us take two hyper-nuclei with different masses, (A_1, Z_1, H) and (A_2, Z_2, H), together with nuclei which differ from them only by one Λ hyperon. When we consider the double ratio (DR) of $Y_{A_1,Z_1,H}/Y_{A_1-1,Z_1,H-1}$ to $Y_{A_2,Z_2,H}/Y_{A_2-1,Z_2,H-1}$ we obtain from the above formulae

$$DR_{A_1A_2} = \frac{Y_{A_1,Z_1,H}/Y_{A_1-1,Z_1,H-1}}{Y_{A_2,Z_2,H}/Y_{A_2-1,Z_2,H-1}} = \alpha_{A_1A_2}\exp\left[-\frac{1}{T}\left(\Delta E^{bh}_{A_1A_2}\right)\right], \qquad (6)$$

where

$$\Delta E^{bh}_{A_1A_2} = E^{bh}_{A_1} - E^{bh}_{A_2}, \qquad (7)$$

and the ratio of the C-coefficients we denote as

$$\alpha_{A_1A_2} = C_{A_1,Z_1,H}/C_{A_2,Z_2,H} . \qquad (8)$$

As one can see from eq.(6), the logarithm of the double ratio is directly proportional to the difference of the hyperon binding energies in A_1 and A_2 hypernuclei, $\Delta E^{bh}_{A_1A_2}$, divided by temperature. Therefore, we can finally rewrite the relation between the hypernuclei yield ratios and the hyperon binding energies as

$$\boxed{\Delta E^{bh}_{A_1A_2} = T \cdot \left[ln(\alpha_{A_1A_2}) - ln(DR_{A_1A_2})\right] . } \qquad (9)$$

$$\Delta E_{bh} = T \cdot \left[ln\left(\frac{(g_{A_1,Z_1,H}/g_{A_1-1,Z_1,H-1})\cdot(A_1^{3/2}/(A_1-1)^{3/2})}{(g_{A_2,Z_2,H}/g_{A_2-1,Z_2,H-1})\cdot(A_2^{3/2}/(A_2-1)^{3/2})}\right) - ln\left(\frac{Y_{A_1,Z_1,H}/Y_{A_1-1,Z_1,H-1}}{Y_{A_2,Z_2,H}/Y_{A_2-1,Z_2,H-1}}\right)\right] .$$
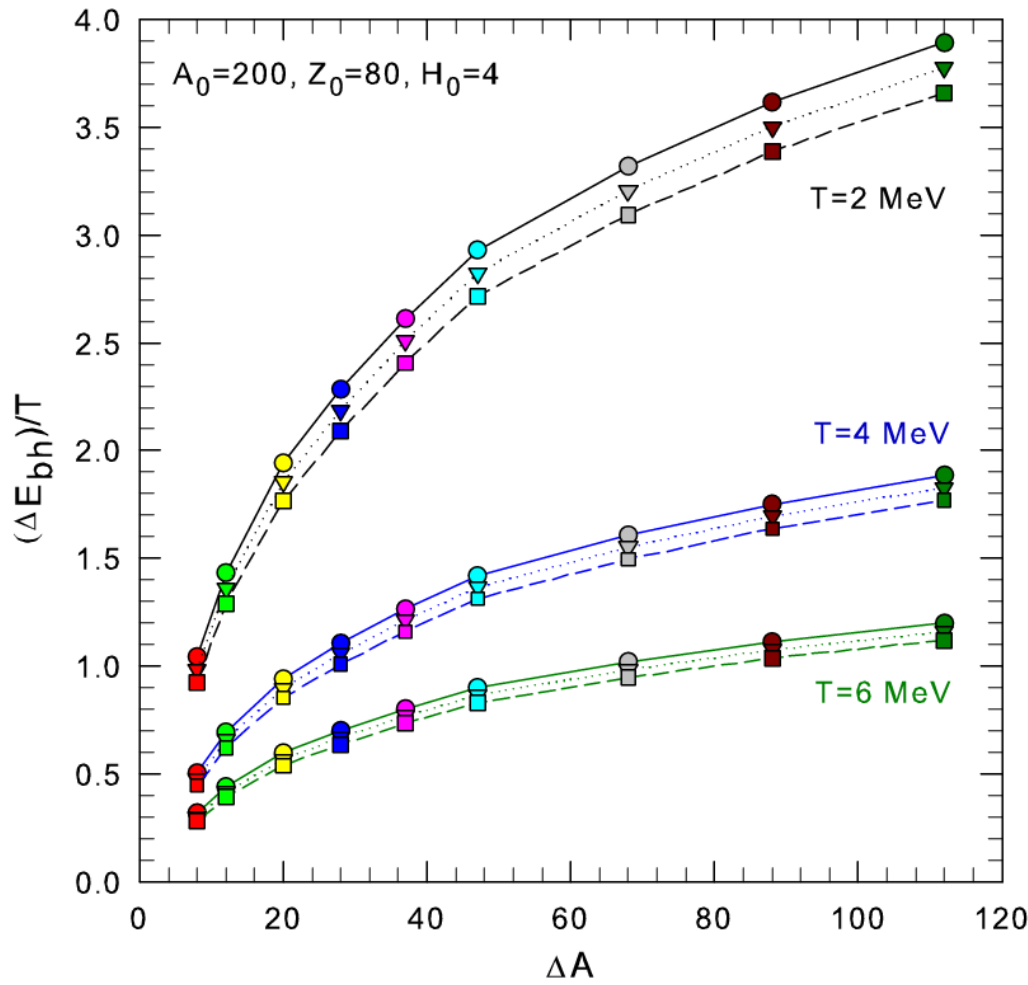
Figure1

The difference of binding energies of hyperons in nuclei extracted from the double yield ratio (ΔE_{bh}) divided by the temperature T versus the mass number difference of these nuclei ΔA, as calculated with the statistical model at different temperatures relevant for multifragmentation reactions.

Baryon composition and temperatures (for groups of curves) of the initial system are given in the figure.

Plot annotations:
- $A_0=200$, $Z_0=80$, $H_0=4$
- y-axis: $(\Delta E_{bh})/T$
- x-axis: ΔA
- T=2 MeV
- T=4 MeV
- T=6 MeV

single

- $(^{13}_{\Lambda}C/^{12}C)/(^{21}_{\Lambda}O/^{20}O)$
- $(^{13}_{\Lambda}C/^{12}C)/(^{25}_{\Lambda}Mg/^{24}Mg)$
- $(^{13}_{\Lambda}C/^{12}C)/(^{33}_{\Lambda}P/^{32}P)$
- $(^{13}_{\Lambda}C/^{12}C)/(^{41}_{\Lambda}S/^{40}S)$
- $(^{13}_{\Lambda}C/^{12}C)/(^{50}_{\Lambda}Ca/^{49}Ca)$
- $(^{13}_{\Lambda}C/^{12}C)/(^{60}_{\Lambda}Cr/^{59}Cr)$
- $(^{13}_{\Lambda}C/^{12}C)/(^{81}_{\Lambda}Ge/^{80}Ge)$
- $(^{13}_{\Lambda}C/^{12}C)/(^{101}_{\Lambda}Zr/^{100}Zr)$
- $(^{13}_{\Lambda}C/^{12}C)/(^{125}_{\Lambda}Sn/^{124}Sn)$

double

- $(^{13}_{\Lambda\Lambda}C/^{12}_{\Lambda}C)/(^{21}_{\Lambda\Lambda}O/^{20}_{\Lambda}O)$
- $(^{13}_{\Lambda\Lambda}C/^{12}_{\Lambda}C)/(^{25}_{\Lambda\Lambda}Mg/^{24}_{\Lambda}Mg)$
- $(^{13}_{\Lambda\Lambda}C/^{12}_{\Lambda}C)/(^{33}_{\Lambda\Lambda}P/^{32}_{\Lambda}P)$
- $(^{13}_{\Lambda\Lambda}C/^{12}_{\Lambda}C)/(^{41}_{\Lambda\Lambda}S/^{40}_{\Lambda}S)$
- $(^{13}_{\Lambda\Lambda}C/^{12}_{\Lambda}C)/(^{50}_{\Lambda\Lambda}Ca/^{49}_{\Lambda}Ca)$
- $(^{13}_{\Lambda\Lambda}C/^{12}_{\Lambda}C)/(^{60}_{\Lambda\Lambda}Cr/^{59}_{\Lambda}Cr)$
- $(^{13}_{\Lambda\Lambda}C/^{12}_{\Lambda}C)/(^{81}_{\Lambda\Lambda}Ge/^{80}_{\Lambda}Ge)$
- $(^{13}_{\Lambda\Lambda}C/^{12}_{\Lambda}C)/(^{101}_{\Lambda\Lambda}Zr/^{100}_{\Lambda}Zr)$
- $(^{13}_{\Lambda\Lambda}C/^{12}_{\Lambda}C)/(^{125}_{\Lambda\Lambda}Sn/^{124}_{\Lambda}Sn)$

triple

- $(^{13}_{3\Lambda}C/^{12}_{\Lambda\Lambda}C)/(^{21}_{3\Lambda}O/^{20}_{\Lambda\Lambda}O)$
- $(^{13}_{3\Lambda}C/^{12}_{\Lambda\Lambda}C)/(^{25}_{3\Lambda}Mg/^{24}_{\Lambda\Lambda}Mg)$
- $(^{13}_{3\Lambda}C/^{12}_{\Lambda\Lambda}C)/(^{33}_{3\Lambda}P/^{32}_{\Lambda\Lambda}P)$
- $(^{13}_{3\Lambda}C/^{12}_{\Lambda\Lambda}C)/(^{41}_{3\Lambda}S/^{40}_{\Lambda\Lambda}S)$
- $(^{13}_{3\Lambda}C/^{12}_{\Lambda\Lambda}C)/(^{50}_{3\Lambda}Ca/^{49}_{\Lambda\Lambda}Ca)$
- $(^{13}_{3\Lambda}C/^{12}_{\Lambda\Lambda}C)/(^{60}_{3\Lambda}Cr/^{59}_{\Lambda\Lambda}Cr)$
- $(^{13}_{3\Lambda}C/^{12}_{\Lambda\Lambda}C)/(^{81}_{3\Lambda}Ge/^{80}_{\Lambda\Lambda}Ge)$
- $(^{13}_{3\Lambda}C/^{12}_{\Lambda\Lambda}C)/(^{101}_{3\Lambda}Zr/^{100}_{\Lambda\Lambda}Zr)$
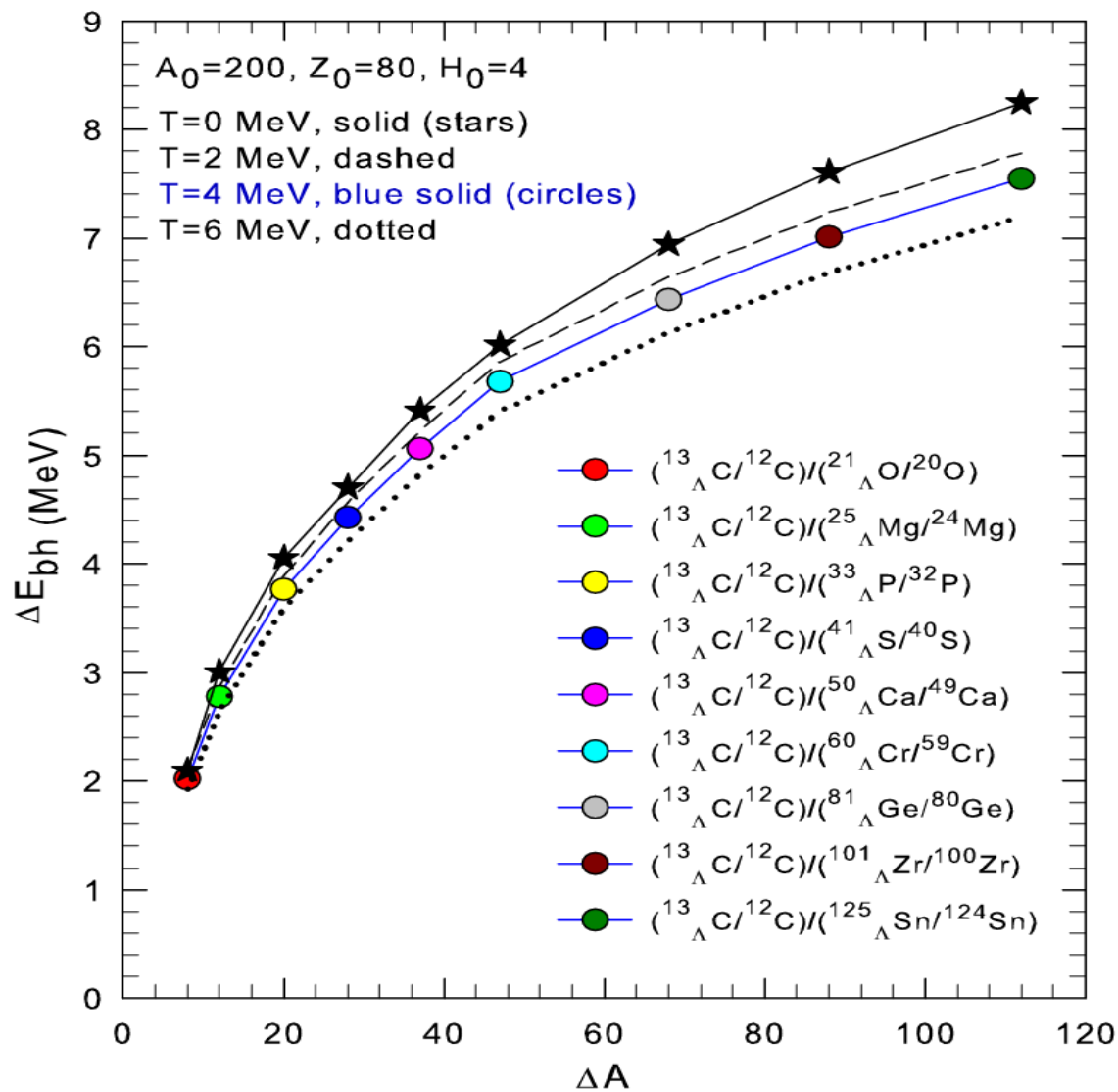- $(^{13}_{3\Lambda}C/^{12}_{\Lambda\Lambda}C)/(^{125}_{3\Lambda}Sn/^{124}_{\Lambda\Lambda}Sn)$

Figure2

The difference of binding energies of hyperons in nuclei (ΔEbh) versus the mass number difference of these nuclei ΔA for single hypernuclei, The statistical calculations are performed involving the double ratio yields shown in the figure for temperatures T=2 MeV (dashed line), 4 MeV (solid line with circle symbols), and 6 MeV (dotted line). The stars (thick line) are the direct calculation of Δebh according to the adopted hyperfragment formula at T=0 and V →∞
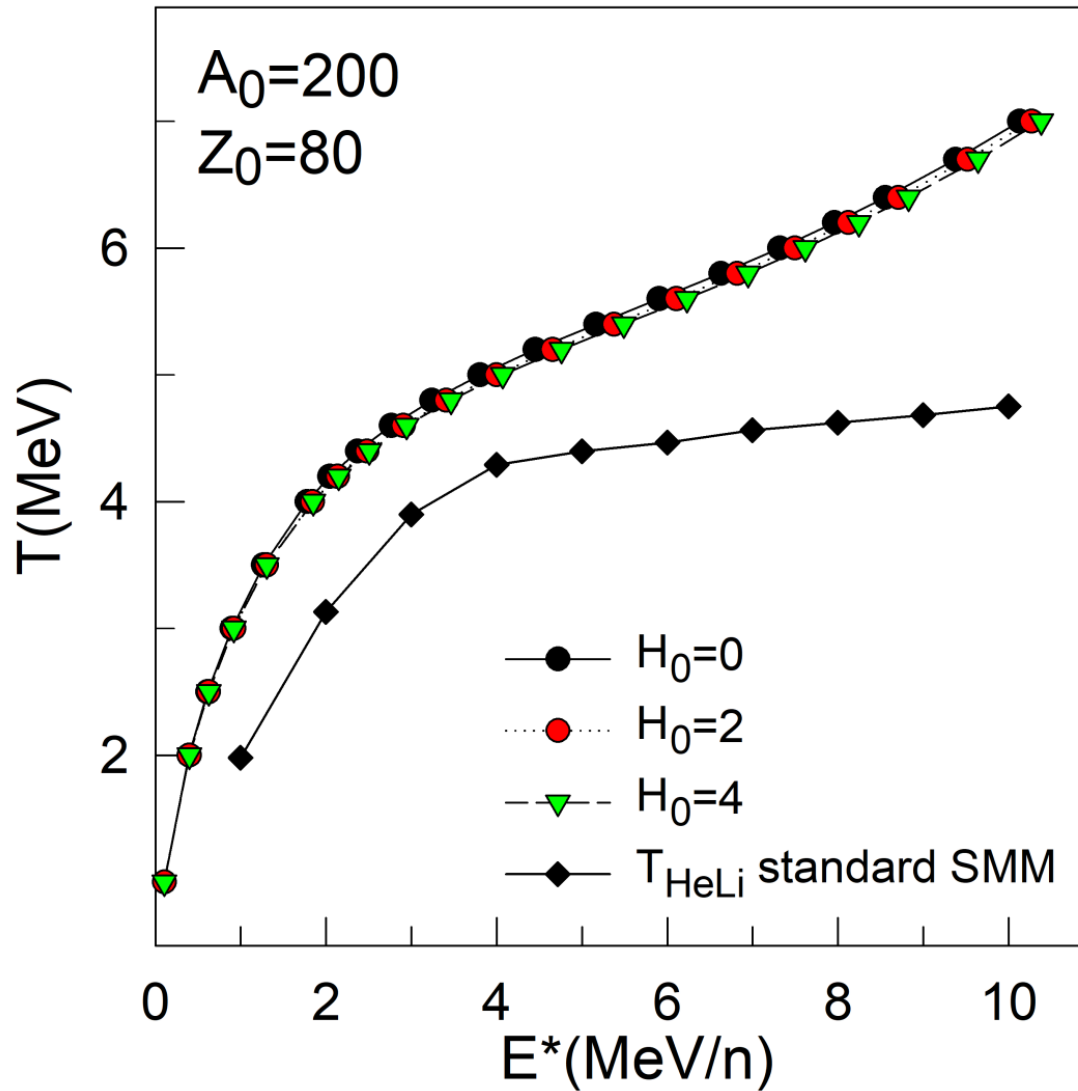
Figure3

The temperature versus the excitation energy for the disintegration of the hypernuclear system with parameters given in the figure. The statistical calculations including different initial numbers of hyperons (0, 2, and 4) are shown by different symbols and lines. The helium-lithium isotope temperature calculated within the standard multifragmentation model are represented by diamonds.
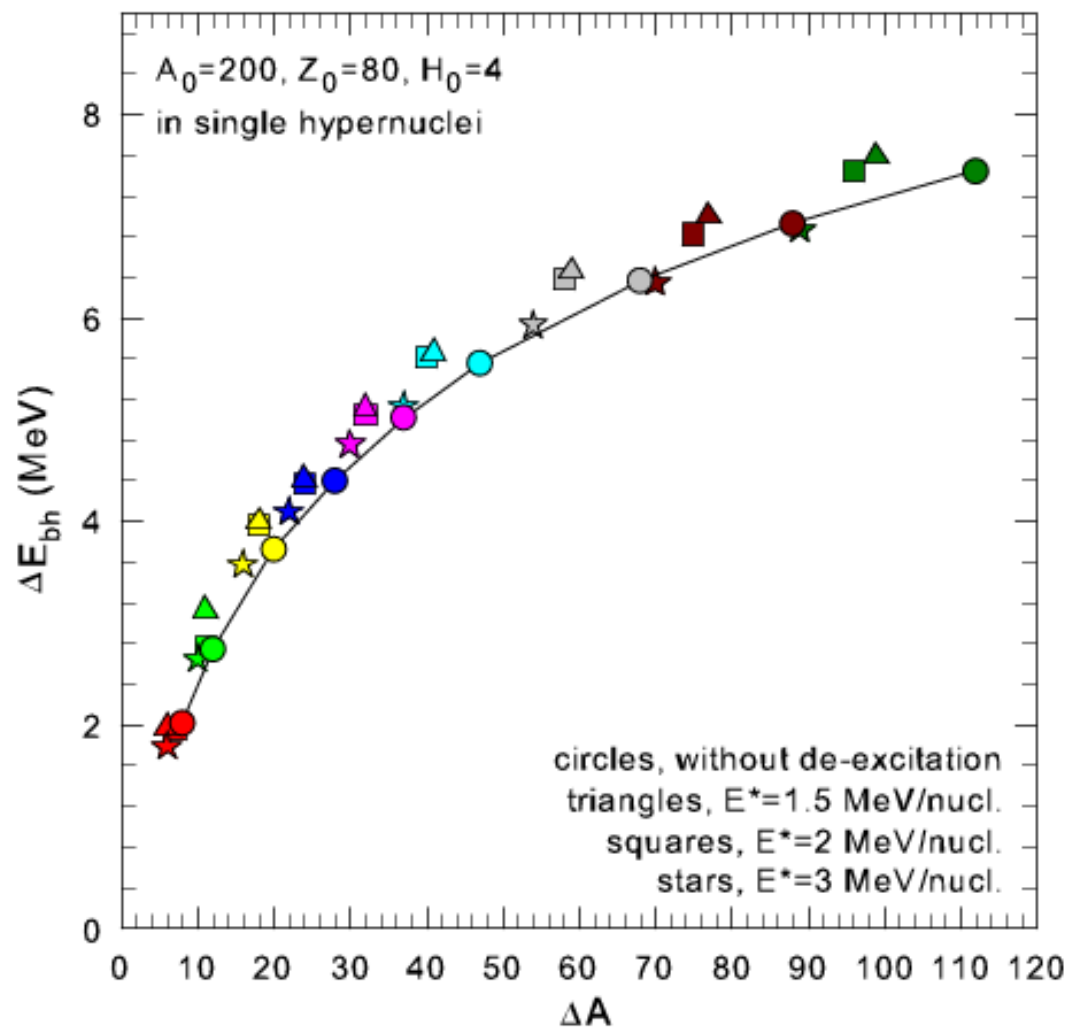
Figure4

Influence of the secondary deexcitaiton on the difference of binding energies of hyperons in nuclei (ΔEbh) as function of their mass number difference of ΔA by taking single hypernuclei (which are the same as in Fig. 2.). The calculations of double ratio yields for primary hot nuclei are shown for temperature 4 MeV (solid line, color circle symbols). Triangles, squares, and stars stand for the calculations with modified double ratios after the secondary deexcitation (via nuclear evaporation) of primary nuclei at excitation energies of 1.5, 2, and 3 MeV/nucleon, respectively. The same color symbols show the modification of ΔEbh and ΔA after the deexcitation evolution of many nuclei leading to the same daughter ones.
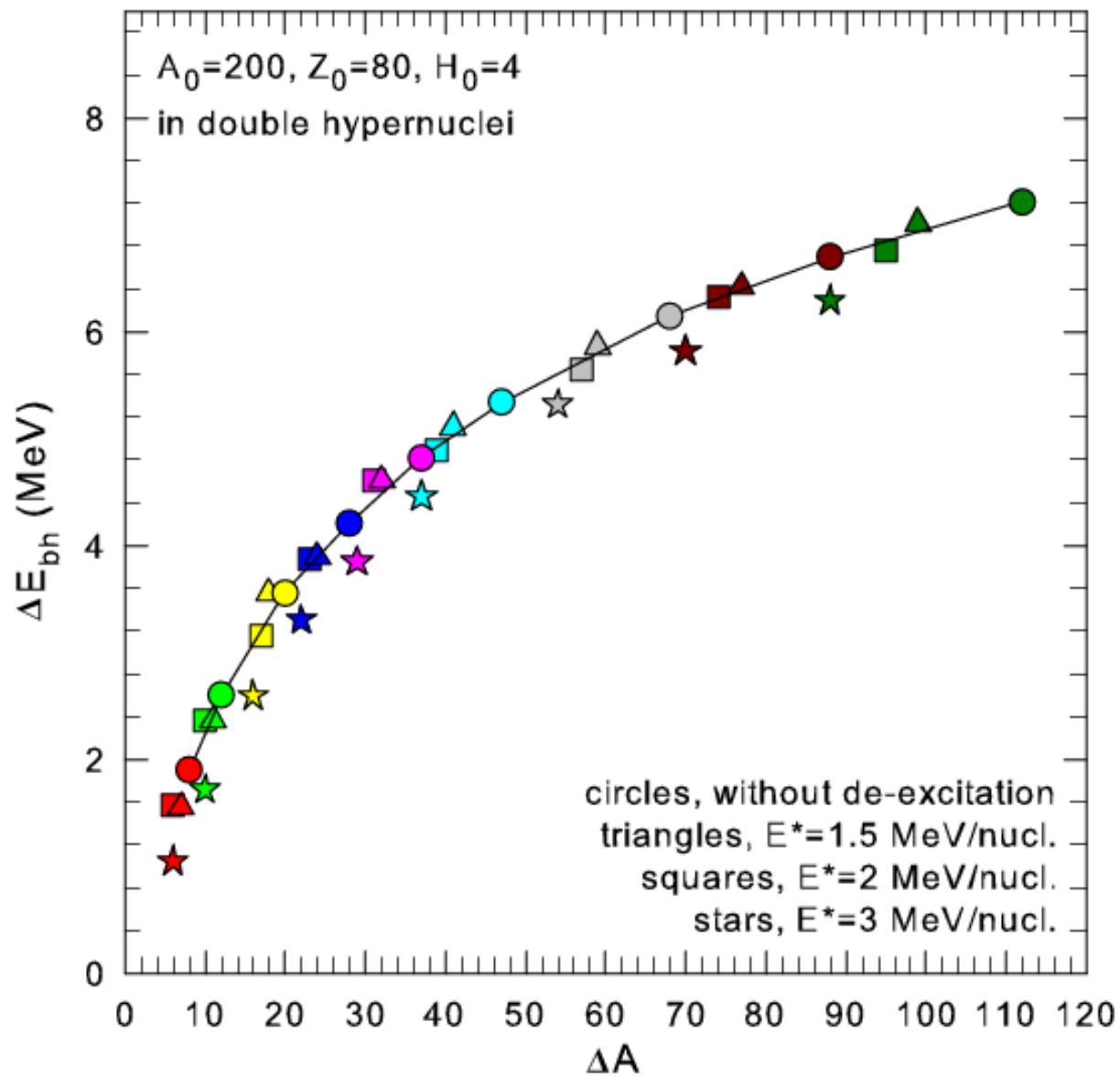
FIG. 5. The same as in Fig. 4, however, for double hypernuclei

Summary

We have investigated the evaporation and fission of middle and heavy hypernuclei since they were not considered up to now because of scarce experimental data [H. Ohm et al., Phys. Rev. C 55, 3062 (1997)]

It is demonstrated that the hyperon binding energies can be effectively evaluated from the yields of different isotopes of hypernuclei. The advantage of double ratio method is its universality and the possibility to involve many different isotopes. This method can also be applied for multi-strange nuclei, which binding energies were very difficult to measure in previous hypernuclear experiments.

We believe such kind of research would be possible at the new generation of ion accelerators of intermediate energies, as FAIR (Darmstadt), NICA (Dubna), and others. It is promising that new advanced experimental installations for the fragment detection will be available soon.

References
[1] Buyukcizmeci N. et al Phys. Rev C **98**, 064603 (2018), Eur. Phys. J. A 55:2 (2019)
[2] Botvina A.S et al., Phys. Rev. C **94**, 054615 (2016).
[3] Buyukcizmeci N., Botvina A.S., Pochodzalla, J., Bleicher, M., Phys. Rev. C 88, 014611 (2013).
[4] Botvina A.S and Pochodzalla, J., Phys. Rev. C 76, 024909 (2007).